

# Cost-benefit analysis of coastal flood defence measures in the North Adriatic Sea

Mattia Amadio<sup>1</sup>, Arthur H. Essenfelder<sup>1</sup>, Stefano Bagli<sup>2</sup>, Sepehr Marzi<sup>1</sup>, Paolo Mazzoli<sup>2</sup>, Jaroslav Mysiak<sup>1</sup>, Stephen Roberts<sup>3</sup>

<sup>1</sup> Centro Euro-Mediterraneo sui Cambiamenti Climatici, Università Ca' Foscari Venezia, Italy

<sup>2</sup> Gecosistema, Rimini, Italy

<sup>3</sup> The Australian National University, Canberra, Australia

Correspondence to: Arthur H. Essenfelder ([arthur.essenfelder@cmcc.it](mailto:arthur.essenfelder@cmcc.it))

## Abstract

The combined effect of ~~extreme global~~ sea levels ~~rise~~ and land subsidence phenomena poses a major threat to coastal settlements. Coastal flooding events are expected to grow in frequency and magnitude, increasing the potential economic losses and costs of adaptation. In Italy, a large share of the population and economic activities are located along ~~the coast of the peninsula, although risk of inundation is not uniformly distributed.~~ ~~The~~ ~~the~~ low-lying coastal plain of ~~Northeast the North Adriatic coast, one of Italy is~~ the most sensitive to relative sea level changes. Over the last half a century, ~~this stretch of e entire north eastern Italian coast~~ has experienced a significant rise in relative sea level, the main component of which was land subsidence; ~~in~~ in the forthcoming decades, climate-induced sea level rise is expected to become the first driver of coastal inundation hazard. We propose an assessment of flood hazard and risk linked with extreme sea level scenarios, both under historical conditions and sea level rise projections at 2050 and 2100. We run a hydrodynamic inundation model on two pilot sites located ~~in the North Adriatic Sea along the North Adriatic the coast of~~ Emilia-Romagna ~~coast~~. Rimini and Cesenatico. Here, we compare alternative ~~extreme sea level risk~~ scenarios accounting for the effect of planned and hypothetical seaside renovation projects against the historical baseline. We apply a flood damage model ~~developed for Italy~~ to estimate the potential economic damage linked to flood scenarios and we calculate the change in expected annual damage according to changes in the relative sea level. Finally, damage reduction benefits are evaluated by means of cost-benefit analysis. Results suggest an overall profitability of the investigated projects over time, with increasing benefits due to increased probability of intense flooding in the next future.

**Key-words:** coastal inundation; ~~Italy~~; extreme sea level; ~~sea level~~ ~~rise~~; cost-benefit analysis; ANUGA; Italy

**Abbreviations:** MSL (Mean Sea Level); TWL (Total Water Level); ESL (Extreme Sea Level); SLR (Sea Level Rise); VLM (Vertical Land Movements); DTM (Digital Terrain Model); EAD (Expected Annual Damage)

## 1. Introduction

Globally, more than 700 million people live in low-lying coastal areas (McGranahan et al., 2007), and about 13% of them are exposed to a 100-year return period flood event (Muis et al., 2016). On average, one million people located in coastal areas are flooded every year (Hinkel et al., 2014). Coastal flood risk shows an increasing trend in many places due to socio-economic growth (Jongman et al., 2012b; Bouwer, 2011) and land subsidence (Nicholls and Cazenave, 2010; Syvitski et al., 2009), but in the near future sea level rise (SLR) will likely be the most important driver of increased coastal inundation risk (Hallegatte et al., 2013; Hinkel et al., 2014). Evidences show that global sea level has risen at faster rates in the past ~~two centuries~~ ~~centuries~~ compared to the millennial trend (Church and White, 2011; Kemp et al., 2011), topping 3.62 mm per year in the last decade ~~(2006-2015)~~ ~~s~~ mainly due to ocean thermal expansion and glacier melting processes (Meyssignac and Cazenave, 2012; Mitchum et al., 2010; Pörtner et al., 2019). According to the IPCC projections, it is very likely

that, by the end of the 21st century, the SLR rate will exceed that observed in the period 1971-2010 for all Representative Concentration Pathway (RCP) scenarios (Pörtner et al., 2019); yet the local sea level can have a strong regional variability, with some places experiencing significant deviations from the global mean change (Stocker et al., 2013). This is particularly worrisome in regions where small changes in the mean sea level (MSL) ~~are more pronounced, considering that even small increases of MSL~~ can drastically change the frequency of extreme sea level (ESL) events, leading up to situations where a 100-year event may occur several times per year by 2100 (Vousdoukas et al., 2018, 2017; Carbognin et al., 2009, 2010; Kirezci et al., 2020). Changes in the frequency of extreme events are likely to make existing coastal protection inadequate in many places, causing a large part of the European coasts to be exposed to flood hazard. Under these premises, coastal floods threaten to trigger devastating impacts on human settlements and activities (McInnes et al., 2003; Lowe et al., 2001; Vousdoukas et al., 2017). In this context, successful coastal risk mitigation and adaptation actions require accurate and detailed information about the characterisation of coastal flood hazard and the performance of ~~alternative~~ coastal defence options. Cost-benefit analysis (CBA) is widely used to evaluate the economic desirability of a disaster risk reduction (DRR) project (Jonkman et al., 2004; Price, 2018; Mechler, 2016). ~~CBA~~ helps decision-makers in evaluating the efficacy of different adaptation options (Kind, 2014; Bos and Zwaneveld, 2017).

In this study, we estimate the benefits of coastal renovation projects along the coast of Emilia-Romagna region (Italy) in terms of avoided economic losses from ESL inundation events under both current and future conditions. ~~To do that, a range of hazard scenarios associated with ESL events are simulated over the two case study. We select two coastal cities as case study areas:~~ i) Rimini, a touristic hotspot that is currently implementing a seafront renovation project; and ii) Cesenatico, a coastal city that could benefit from similar measures in addition to existing defence mechanisms. ~~We design worst case scenarios of ESL resulting from the combination of the maximum levels of mean sea level, vertical land movement, storm surge, tide, and wave setup to verify the effectiveness of the above mentioned coastal defence structures in reducing flood hazard and related impacts over the urban area. To do that, The scenarios are designed by combining probabilistic data from historical ESL events, with the estimates of relative mean sea level (RMSL) MSL change for those locations. RMSL change accounts for both the eustatic global rise and the locally measured vertical land movement effect. Each scenario is translated-evaluated in terms of direct economic impacts over residential areas using a locally-calibrated flood damage model. The combination of different risk scenarios in a CBA framework allows to evaluate the economic benefits-profitability brought by the project implementation in terms of avoided direct flood losses up to the end of the century.~~

## 2. Area of study

Located in the central Mediterranean Sea, the Italian peninsula has more than 8,300 km of coast lines, hosting around 18% of the country population, numerous towns and cities, industrial plants, commercial harbours and touristic activities, as well as cultural and natural heritage sites. Existing country-scale estimates of SLR impacts up to the end of this century helps to identify the most critically exposed coastal areas of Italy (Antonioli et al., 2017; Marsico et al., 2017; Bonaduce et al., 2016; Lambeck et al., 2011). About 40% of the country's coastal perimeter consist of a flat ~~coastal~~ profile (ISPRA, 2012), potentially more vulnerable to the impacts of ESL events. The North Adriatic coastal plain is ~~acknowledged to be~~ the largest and most vulnerable location to extreme coastal events due to the shape, morphology and low bathymetry of the Adriatic sea basin, which cause water level to increase relatively fast during coastal storms (Perini et al., 2017; Ciavola and Coco, 2017; Carbognin et al., 2010). ~~Here~~ The ESL here is driven mainly by astronomical tide, ranging about one meter in the northernmost sector; and by meteorological forcing, such as low pressure, seiches and prolonged

Field Code Changed

rotational wind systems, which are the main trigger of storm surge ~~in the Adriatic basin~~ (Vousdoukas et al., 2017; Umgiesser et al., 2020). In addition to that, all the coastal profile of the Padan plain shows relatively fast subsiding rates, partially due to natural phenomena, but in large part linked to human activities (Perini et al., 2017; Carbognin et al., 2009; Meli et al., 2020). As a contributing factor to coastal flood risk, the intensification of urbanization has led to increased exposure along the Adriatic coast during the last 50 years, with many regions building over half of the available land within 300 meters from the shoreline (ISPRA, 2012). Figure 1 shows the location of the two case study areas, Cesenatico and Rimini, along with land-cover maps showing the position of coastal defences accounted in this study.



**Figure 1.** Case-study locations along the Emilia-Romagna coast: Cesenatico and Rimini. The coastal defence structure assessed in this study are shown in black. Buildings' footprint data from Regional Environmental Agency (ARPA) 2020. Basemap © Google Maps 2020.

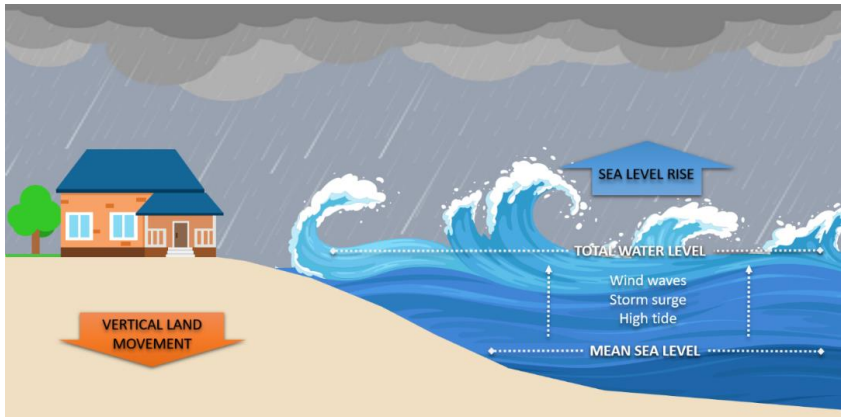
The number of ESL events reported to cause impacts along the Emilia-Romagna coast shows a steady increase since the second half of the past century (Perini et al., 2011); ~~this, which is in part partially~~ explained by to the socio-economic development, ~~which increased the of the coast exposing increasing extent of built-up~~ asset ~~potentially exposed~~ to flood risk. The landscape along the 130 km regional coastline is almost ~~completely~~ flat, the only relief being old beach ridges, artificial embankments and a small number of dunes. The coastal perimeter is delineated by a wide sandy beach that is generally protected by offshore breakwaters, groins and jetties. The land elevation is often close to (or even below) the MSL, while the coastal corridor is heavily urbanised. Cesenatico has about 26,000 residents, while Rimini has 150,000. The towns have a strong touristic vocation, hosting large beach resort and bathing facilities along the beach and hundreds of hotels and rental housing located just behind the seaside. Both places have been affected by coastal storms resulting in flooding of buildings and activities, beach erosion and regression of the coastline. -The most recent inundation events were observed in March 2010, November 2012 and February 2015. The 2015 event was one of the most severe ever recorded, with ESL values corresponding to a probability ~~(return period)~~ of once in 100 years. It caused severe damages along the whole regional coast and, in some locations, required the evacuation of people from their houses; many buildings and roads were covered by sand brought by the flood wave; touristic

112 infrastructures near the shore were seriously damaged, and some port channels overflowed the surrounding  
113 areas. The economic impact of the event was estimated topping 7.5 M Eur (Perini et al., 2015).

114 **3. Methodology**

115 **3.1 Components of the analysis**

116 Coastal inundation is caused by an increase of total water level (TWL), most often associated to extreme sea  
117 level (ESL) events, which are often generated by a combination of high astronomical tide and meteorological  
118 drivers such as storm surge and wind waves (Figure 2). Probabilistic flood risk assessments  
119 under of scenarios often generally consider ESL as the result of the combined effects of the contributions from  
120 storm surge and tides to design the ESL scenarios (Muis et al., 2015; Vousdoukas et al., 2017). More recent  
121 studies were able to also account also for the combined effects of storm tides and for the effects of waves by  
122 either adding wave setup to the ESL or by simulating the dynamics of breaking waves on the coast (Kirezci et  
123 al., 2020; Melet et al., 2020; Li et al., 2020; Wang et al., 2021; Muis et al., 2020; Lionello et al., 2021; McInnes et  
124 al., 2009; Idier et al., 2019). In our study, we consider ESL-TWL near shore as the result of the combination of  
125 high tide, storm surge, and wave setup.



126 **Figure 2.** Components of the analysis for extreme sea level events: total water level is the sum of maximum  
127 tide, storm surge and wind waves over mean sea level. Vertical land movement and sea level rise affects the  
128 mean sea level on the long run.

130 In order to translate an ESL event into flooding, the identification of areas threatened by coastal flooding  
131 from ESL events is often done by means of flood maps, which are generated through hydrostatic or  
132 hydrodynamic modelling approaches. These approaches differ substantially in their complexity and their  
133 ability to represent environmental processes. The hydrostatic static inundation approach, also  
134 called (e.g. sometimes referred as “bathtub” methods), is methodologically the simplest and computationally  
135 quick, as it does not consider dynamic processes such as flow mass conservation and the effect of land  
136 cover on the spread of floodwater, often assuming flooded all the areas as those with an elevation lower below  
137 than the forcing water level as flooded. It comes with a low computational cost and thus it has been  
138 extensively used for studies of different scales and resolutions to explore coastal flood impact (Hinkel et al.,  
139 2010, 2014; Jongman et al., 2012b; Ramirez et al., 2016; Vousdoukas et al., 2016; Muis et al., 2016). These  
140 assumptions and simplifications often result in substantial overestimation/misestimation of flood extents

Field Code Changed

Field Code Changed

compared to the hydrodynamic flood modelling and observations (Bates et al., 2005; Vousdoukas et al., 2016; Breilh et al., 2013; Ramirez et al., 2016; Seenath et al., 2016; Kumbier et al., 2019; Anderson et al., 2018). When solely utilised for supporting community resilience planning to SLR, static inundation methods may arguably pose threats to coastal infrastructure, communities, and ecosystems (Anderson et al., 2018). Additionally, static models assume that flood propagation is only limited by topography and that maximum storm tide water levels are maintained for an infinite duration. These assumptions and simplifications often result in substantial overestimation of the flood extents compared to hydraulic modelling and observations (Bates et al., 2005; Vousdoukas et al., 2016; Breilh et al., 2013; Ramirez et al., 2016; Seenath et al., 2016; Kumbier et al., 2019).

To overcome these limitations, coastal hazard management moved towards more advanced hydrodynamic flood modelling approaches that could be capable of accounting for the effects of wind, waves, tide, current, and river run-off and can be used (Barnard et al., 2019). The most advanced models can simulate atmospheric-ocean-land interactions from the deep ocean to the coast with a high predictive skill (Bates et al., 2005; Seenath et al., 2016; Vousdoukas et al., 2016; Lewis et al., 2013), at the costs of a more complex model setup, extensive data requirements for various high resolution input datasets and significantly longer computational times (Teng et al., 2017). As an intermediate solution, simplified 2D hydrodynamic flood models that focus on nearshore processes have been developed which are capable of reducing the computational cost while taking into consideration either only water mass conservation (Breilh et al., 2013), aspects of flooding hydrodynamics (Dottori et al., 2018) or the presence of obstacles (Perini et al., 2016). Although they reduce the complexity of the physical processes, they have been proven to be reliable for coastal flooding applications, such as the reproduction of coastal flooding due to storm-tide events (Ramirez et al., 2016; Bates et al., 2005; Skinner et al., 2015; Smith et al., 2012).

In this study, estimates of ESL components (storm surge, tides and waves) are obtained for the North Adriatic up to year 2100 by combining reference hazard scenarios derived from the analysis of historical records (Perini et al., 2011, 2016, 2017; Armaroli et al., 2012; Armaroli and Duo, 2018) with regionalised projections of SLR (Vousdoukas et al., 2017) and local vertical land movements (VLM) rates (Perini et al., 2017; Carbognin et al., 2009). On this basis, four hypothetical ESL scenarios are designed, ranging from low intensity-high frequency to high intensity-low frequency, under namely once in 1, 10, 100 and 250 years, are considered both current and future (2050 and 2100) conditions. The 2D hydrodynamic model ANUGA (Roberts et al., 2015) is applied to simulate the inundation of land areas during ESL accounting for individual components (storm surge, tides and waves). Land morphology and exposure of coastal settlements are described by high-resolution DTM (LiDAR) and bathymetry, in combination with land use and buildings footprints. The effect of hazard mitigation structures (both designed and under construction) are explicitly accounted by the model in the “defended” simulation scenario, in contrast to the baseline scenario, where only existing defence structures (groins, jetties, breakwaters and sand dunes) are accounted.

### 3.3.2 Vertical Land Movement

Vertical land movements result from a combination of slow geological processes such as tectonic activity and glacial isostatic adjustment (Peltier et al., 2015; Peltier, 2004), and medium-term phenomena, such as sediment loading and soil compaction (Carminati and Martinelli, 2002; Lambeck and Purcell, 2005). The latter can greatly oversize geological processes at local scale (Wöppelmann and Marcos, 2012); in particular, faster subsidence occurs in presence of intense anthropogenic activities such as water withdrawal and natural gas

184 extraction (Teatini et al., 2006; Polcari et al., 2018). Most of the peninsula shows a slow subsiding trend,  
 185 although with some local variability. An estimate of VLM rates due to tectonic activity has been derived from  
 186 studies conducted in Italy (Solari et al., 2018; Antonioli et al., 2017; Marsico et al., 2017; Lambeck et al., 2011).  
 187 The North Adriatic coastal plain shows the most intense long-term geological subsidence rates (about 1 mm  
 188 per year), increasing North to South. Yet in the last decades these rates were often greatly exceeded by ground  
 189 compaction rates observed by multi-temporal SAR Interferometry (Gambolati et al., 1998; Antonioli et al.,  
 190 2017; Polcari et al., 2018; Solari et al., 2018). Observed subsidence is about one order of magnitude faster where  
 191 the aquifer system has been extensively exploited for agricultural, industrial and civil use since the post-war  
 192 industrial boom. From the 1970s, however, with the halt of groundwater withdrawals, anthropogenic drivers  
 193 of subsidence has been strongly reduced or stopped (Carbognin et al., 2009). Nonetheless, subsidence still  
 194 continues at much faster rates than expected from natural phenomena (Teatini et al., 2005). Geodetic surveys  
 195 carried out from 1953 to 2003 along the Ravenna coast provide evidence of a cumulative land subsidence  
 196 exceeding 1 m at some sites due to gas extraction activities. Average subsidence rates observed for 2006-2011  
 197 along the Emilia-Romagna coast are around 5 mm/yr, exceeding 10 mm/yr in the back shore of the Cesenatico  
 198 and Rimini areas and topping 20-50 mm/yr in Ravenna (Perini et al., 2017; Carbognin et al., 2009). Based on  
 199 these current rates, we assume an average fixed annual VLM of 5 mm in both Cesenatico and Rimini up to the  
 200 end of the century. This remarkable difference between natural VLM rates and observations would produce a  
 201 dramatic effect on the estimated SLR scenarios: at present rates, Rimini would see an increase of MSL by 0.15  
 202 m in 2050 and more than 0.4 m in 2100 independently from eustatic SLR. Since these rates are connected with  
 203 human activity, it is not possible to foresee ~~exactly~~ how they will change in the longer ~~term~~ run.

#### 204 **3.43.3 Sea Level Rise**

205 The long availability of tide gauge data along the North Adriatic coast allows to assess the eustatic changes in  
 206 MSL during the last century, estimated to be  $\pm 1.3$  mm/year (Scarascia and Lionello, 2013). This is consistent  
 207 with published values for the Mediterranean Sea (Tsimplis et al., 2008; Tsimplis and Rixen, 2002) and the  
 208 Adriatic Sea (Tsimplis et al., 2012; Carbognin et al., 2009) Records from the gauge station of Marina di Ravenna  
 209 show an eustatic rise of 1.2 mm per year from 1890 to 2007, in good agreement with the eustatic rise measured  
 210 at other stations in the Mediterranean Sea. The projections of future MSL account for sea thermal expansions  
 211 from four global circulation models, estimated contributions from ice-sheets and glaciers (Hinkel et al., 2014)  
 212 and long-term subsidence projections (Peltier, 2004). The ensemble mean is chosen to represent each RCP for  
 213 different time slices. The increase in the central Mediterranean basin is projected to be approximately 0.2 m by  
 214 2050 and between 0.5 and 0.7 m by 2100, compared to historical mean (1970-2004) (Vousdoukas et al., 2017).  
 215 As agreed with local stakeholders (Comune di Rimini), our analysis considers the intermediate emission  
 216 scenario RCP 4.5, projecting an increase in MSL of 0.53 m at 2100. It must be noted that these projections,  
 217 although downscaled for the Adriatic basin, do not account for the peculiar continental characteristics of the  
 218 shallow northern Adriatic sector, where the hydrodynamics and oceanographic parameters partially depend  
 219 on the freshwater inflow (Zanchettin et al., 2007).

#### 220 **3.53.4 Tides and meteorological forcing**

221 Storm surge and wind waves represent the largest contribution to TWL during an ESL event. An estimation  
 222 of these components is obtained for the two coastal sites from the analysis of tide gauge and buoy records,  
 223 and from the description of historical extreme events presented in local studies (Armaroli and Duo, 2018;  
 224 Perini et al., 2012; Masina et al., 2015; Perini et al., 2011, 2017). This area is microtidal: the mean neap tidal  
 225 range is 30–40 cm, and the mean spring tidal range is 80–90 cm. Most storm surge events have a duration of  
 226 less than 24 h and a maximum significant wave height of about 2.5 m. During extreme cyclonic events, the

Field Code Changed



sequence of SE wind (*Sirocco*) piling the water North and E-NE wind (*Bora*) pushing waves towards the coast can generate severe inundation events, with significant wave height ranging 3.3 – 4.7 m and exceptionally exceeding 5.5 m (Armaroli et al., 2012). Fifty significant events have been recorded from 1946 to 2010 on the ER coast, with half of them causing severe impacts along the whole coast and 10 of them being associated with important flooding events (Perini et al., 2017). The most severe events are found when strong winds blow during exceptional tide peaks, most often happening in late autumn and winter. The event of November 1966 represents the highest ESL on records, causing significant impacts along the regional coast: the recorded water level was 1.20 m above MSL, and wave heights offshore were estimated around 6–7 m (Garnier et al., 2018; Perini et al., 2011). The whole coastline suffered from erosion and inundation, especially in the province of Rimini. Atmospheric forcing shown significant variability for the period 1960 onwards (Tsimplis et al., 2012), but there is no strong evidence supporting a significant change in ~~marine trend-storminess frequency or severity~~ for the ~~next-near~~ future (Lionello, 2012; Zanchettin et al., 2020; Lionello et al., 2020, 2017). Thus, ~~in our model~~ we assume ~~the frequency and intensity of meteorological events forcing~~ to remain the same up to 2100.

### 3.6.3.5 Terrain morphology and coastal defence structures

Reliable ~~bathymetries-bathymetry~~ and topography are required in order to run the hydrodynamic modelling at the local scale. Bathymetric data for the Mediterranean Sea were obtained from the European Marine Observation and Data Network (EMODnet) at 100 m resolution. The description of terrain morphology comes from the official high-resolution LIDAR DTM (MATTM, 2019). First, we combined the coastal dataset (2 m resolution and vertical accuracy of  $\pm 0.2$  m), and the inland dataset (1 m resolution and vertical accuracy  $\pm 0.1$  m) into one seamless layer. Then, the DTM is supplemented with geometries of existing coastal protection elements such as jetties, groins and breakwaters obtained from the digital Regional Technical Map. In Rimini, the *Parco del Mare* (Figure 3) is an urban renovation project which aims to improve the seafront promenade: the existing road and parking lots are converted into an urban green infrastructure consisting of a concrete barrier covered by vegetated sandy dunes with walking paths. This project also acts as a coastal defence system during extreme sea level events. The barrier rises 2.8 meters along the southern section of the town, south of the marina; no barrier is planned on the northern coastal perimeter. The *Parco del Mare* project is ~~currently expected to be completed by 2021 under construction~~ and has been taken in account in the evaluation of the “defended” scenarios by adding the barrier ~~elevation~~ to the DTM.



Figure 3. Prototype design of Parco del Mare project in Rimini. Adapted from JDS Architects.

In Cesenatico, the existing defence structures include a moving barrier system (*Porte Vinciane*) located on the port channel, coupled with a dewatering pump which discharge the meteoric waters in the sea. The barriers close automatically if the TWL surpasses 1 meter over the mean sea level, preventing floods in the historical centre up to 2.2 meters of TWL. Additional defence structures include the winter dunes, which consist of a 2.2 meter-tall intermittent, non-reinforced sand barrier. In the defended scenario, we envisage a coastal defence

structure similar to Rimini's *Parco del Mare* project, spanning both North and South of the port channel with a total length of 7.8 km. A proper setup of the inundation model required to first perform The DTM was manually some manual editing of the DTM using based on additional reference data (i.e. on-site observations or aerial photography) in order to remove artefacts and to produce a more n elevation model that realistically representrepresentation of the land morphologymorphology and associated water dynamics (e.g. removal of non-existent sink-holes). Bridges and tunnels are the most critical elements that required DTM correction in order to avoid misrepresentations of the water flow routing.

### 3.7.3.6 Scenario designInundation modelling

In order to design probabilistic nearshore (i.e. boundary conditions to the hydrodynamic model)scenarios associated to ESL of different intensities to use as boundary conditions in the hydrodynamic model, we rely on existing frequency-analysis of storm surgeESL events occurring on the regional coast (Perini et al., 2011, 2016, 2017), which have been adopted by the Regional Environmental Agency to define the official coastal flood hazard zones and related protection standards (ARPA Emilia-Romagna, 2019). The probability of occurrence of these ESL scenarios is expressed in terms of return period (RP), which is the estimated average time interval (in years) between events of similar intensity. Based on that frequency analysis of historical ESL events, fFour scenarios of increasing intensity are designed, namely RP 1, 10, 100 and 250 years. For each of these hypothetical scenarios, the TWL nearshore on the coastland is calculated as the sum of extreme values for storm surge level (SS), max tide (Tmax) and wave setup (Ws) at each time-step. The combined effects of the storm tide and waves can lead to significant damage or destruction to buildings and infrastructure (CITE). Most probabilistic flood risk assessments under climate change scenarios consider the contributions from storm surge and tides to extreme sea level (CITE). More recently, probabilistic flood risk assessments include also the combined effects of storm tides and waves (CITE). We follow recent contributions to probabilistic flood risk assessments by considering waves as an interconnected component of storm surge (CITE). Based on the frequency analysis results adopted by the Regional Environmental Agency of the Emilia Romagna Region (see Table 1). We develop a set of trigonometric equations based on harmonic analysis concepts to characterise the amplitude and period of tidal, storm surge, and wave levels as: the harmonics constituents that describe the theoretical temporal evolution of the nearshore TWL during an ESL event (see Figure 4). Harmonics constituents are the elements in a mathematical expression of a series of periodic terms and have been used in harmonic analysis for sea level prediction since the early 1960s (Boon, 2011; Famikhalili et al., 2020; Fuhrmann et al., 2019; Annunziato and Probst, 2016). The set of equations used in the study are specified in Annex 1, together with sample applications and validation metrics to observed ESL events along the coast of ER. Additional variables to characterize the event dynamics are the storm surge duration (Time, in hours) and the wave period (Wp, in seconds), both -and the event duration (Time, in hours) are obtainedobtained from regional studies of ESL events -from analysis of observations recorded during historical ESL events on the coast of Emilia Romagna from 1946 to 2010 (Perini et al., 2011), matched with the probabilistic distribution of RP scenarios (Armaroli et al., 2012; Armaroli and Duo, 2018). Projections of TWL at 2050 and 2100 are calculated for the same set of RP scenarios by adding SLR and VLM contributions to the MSL, thus shifting the TWL curve up by 33 cm in 2050 and by 97 cm in 2100. In our scenarios, wave direction is set to be oriented perpendicular to the coast.

**Table 1.** components of nearshore TWL for four ESL scenarios (RPs) designed according to analysis of historical ESL events and projected MSL change (2050 and 2100), accounting for both SLR (RCP 4.5) and average VLM rate.

	Extreme event features					Historical	2050			2100		
RP	SS	Tmax	Ws	Time	Wp	TWL	SLR	VLM	TWL	SLR	VLM	TWL

Field Code Changed



(years)	(m)	(m)	(m)	(h)	(s)	(m)	(m)	(m)	(m)	(m)	(m)	(m)
1	0.60	0.40	0.22	32	7.7	1.22	0.14	0.19	1.55	0.53	0.44	2.19
10	0.79	0.40	0.30	42	8.9	1.49	0.14	0.19	1.82	0.53	0.44	2.46
100	1.02	0.40	0.39	55	9.9	1.81	0.14	0.19	2.14	0.53	0.44	2.78
250	1.40	0.45	0.65	75	11	2.50	0.14	0.19	2.83	0.53	0.44	3.47

Our approach is precautionary as it provides worst case TWL values: SS peak is set to coincide with  $T_{max}$  and  $W_s$  at the mid of the event, thus resulting in the maximum TWL possible under that scenario. The scenario RP 250 years makes the upper boundary of hazard intensity, considering all components of TWL to reach their most extreme values and summing up to +2.5 meters over MSL under historical conditions. The TWL is calculated under the same occurrence probability scenarios, projected to 2050 and 2100 by summing up SLR and VLM contributions to the MSL.

we design four synthetic ESL probabilistic scenarios by considering the intensity of waves at any given time as a function of the intensity of  $W_s$  and the SS level, set for coinciding the maximum  $W_s$  level with the timing of maximum storm tide level and following the assumption of worst case scenario, while wave period is specific for each probabilistic scenario. We then estimate the coastal inundation process by making use of a 2D hydrodynamic model while forcing the boundary conditions of the case study areas using the data from the synthetic ESL probabilistic scenarios. Figure 4 shows how TWL is considered during the idealised events for the scenario RP 10 years (additional figures for all RPs can be found in Annex 1). Table 1 summarizes the values for each component considered in the four probability scenarios.

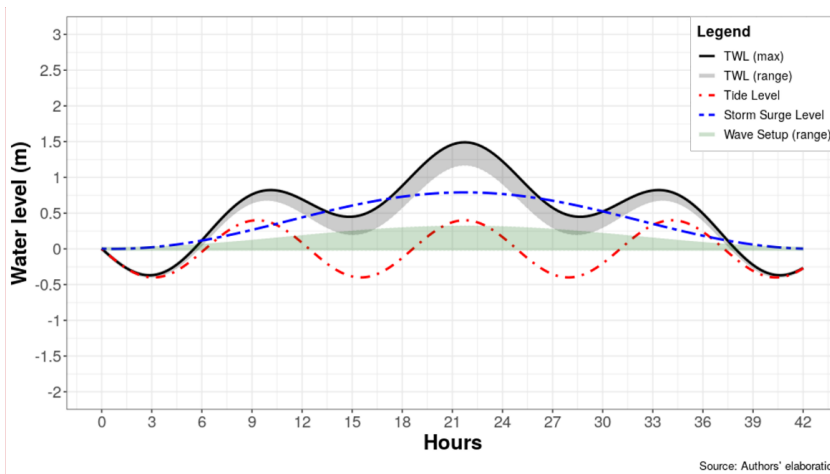


**Figure 4.** Design of dynamic ESL scenario corresponding to RP 10 years under historical MSL conditions using trigonometric functions for RP 10 years. The maximum TWL is shown as the black continuous line, while TWL range at any given time is shown as the shaded grey area. The components of the nearshore TWL as shown in the figure are the tide level (red dashed line), the storm surge level (blue dashed line) and the wave setup (green shaded area). Wave setup is represented as a shaded area due to its high frequency (period of 8.9s). Mean sea level is set as 0 m.a.s.l. for facilitating the visualisation. MSL (0 m). In this scenario (RP 10) the maximum storm surge level is 0.79 m, the maximum high tide is 0.40 m, and the wave setup ranges from 0.00 m to 0.30 m, with a wave period of 8.9 seconds. At the peak of the event, these conditions produce a maximum TWL of 1.49 m. Additional figures for all RPs can be found in Annex 1.

**Commented [MA1]:** Picture was replaced to represent more closely what has been done in the simulation. Previously, the wave component was roughly (and erroneously) simplified in the chart. Now we represent it as it really is accounted in the setup, with a period of few seconds represented by green range, and reflected by the grey range of the TWL.

Figure 5 shows how the nearshore TWL results at any given time from the combination of storm surge, tide level and wave setup in the scenario RP 10 years (additional figures for all RP scenarios can be found in Annex 1). These hypothetical events are designed assuming trigonometric functionals are used to forms describing the a simplified approximation of oscillation dynamic for each component affecting the water level due to the different components defining TWL (Boon, 2011; Famillkhalili et al., 2020; Fuhrmann et al., 2019). The equations describing these functions describing each component are specified in Annex 1.

The individual contribution of  $SS$  and  $T_{max}$  levels are represented by coloured dashed lines in the figure. The  $Ws$  component is shown as a green shaded area due to its high frequency (defined by the wave period,  $Wp$ , in seconds), thus representing the range of values assumed in any given time. The intensity of waves contribution to ESL is and thus the resulting range of  $Ws$  is assumed to grow to its upper boundary proportionally with the increase of the  $SS$  component.  $Wp$  and the event duration ( $Time$ , in hours) are obtained from analysis of observations recorded during historical ESL events on the coast of Emilia Romagna from 1946 to 2010 (Perini et al., 2011), matched with the probabilistic distribution of RP scenarios (Armaroli et al., 2012; Armaroli and Duo, 2018). In our scenarios, wave direction is set to be oriented perpendicular to the coast. The combination of these components (shown as the shaded black area) represents the shaded grey area represents the range of TWL as sum of these components for any given time, while the black continuous line represents the maximum TWL at any given time during the event. Our approach is precautionary as it provides worst-case TWL values:  $SS$  peak is set to coincide with  $T_{max}$  and  $Ws$  at the mid of the event, thus resulting in the maximum TWL possible under each scenario.

Shaded areas indicate the variability (i.e. range) of the free water surface due to the presence of waves. For a RP 10, the maximum storm surge level is 0.79 m, the maximum high tide contribution is 0.40 m, and wave setup ranges from 0.00 m to 0.30 m, with a wave period of 8.9s. At the peak of the event, these conditions produce a maximum TWL of 1.49 m. These hypothetical events are designed assuming trigonometric functional forms describing the oscillation of water level due to the different components defining TWL (Boon, 2011; Famillkhalili et al., 2020; Fuhrmann et al., 2019). The equations describing each component are specified in Annex 1.

Additional details are wave period ( $Wp$ , in seconds) and event duration ( $Time$ , in hours), which are required by the hydrodynamic model to determine the maximum extent of inland water propagation. Both variables are obtained from analysis of observations recorded during historical ESL events on the coast of Emilia Romagna from 1946 to 2010 (Perini et al., 2011), matched with the probabilistic distribution of RP scenarios (Armaroli et al., 2012; Armaroli and Duo, 2018). In our scenarios, wave direction is set to be oriented perpendicular to the coast.

Our approach is precautionary as it provides worst case TWL values: storm surge peak is set to coincide with the tidal peak at the mid of the event, thus resulting in the maximum TWL possible under that scenario. The scenario RP 250 years makes the upper boundary of hazard intensity, considering all components of TWL to reach their most extreme values and cumming up to +2.5 meters over MSL under historical conditions. The TWL is calculated under the same occurrence probability scenarios, projected to 2050 and 2100 by cumming up SLR and VLM contributions to the MSL. Table 1 summarizes the values for each component considered in the four probability scenarios.

Our approach is precautionary as it provides worst case TWL values:  $SS$  peak is set to coincide with  $T_{max}$  and  $Ws$  at the mid of the event, thus resulting in the maximum TWL possible under that scenario. The scenario RP 250 years makes the upper boundary of hazard intensity, considering all components of TWL to reach their most extreme values and cumming up to +2.5 meters over MSL under historical conditions. The TWL is

calculated under the same occurrence probability scenarios, projected to 2050 and 2100 by summing up SLR and VLM contributions to the MSL. We then estimate the coastal inundation process by making use of a 2D hydrodynamic model while forcing the boundary conditions of the case study areas using the data from the synthetic ESL probabilistic scenarios.

### 3.7 Inundation modelling

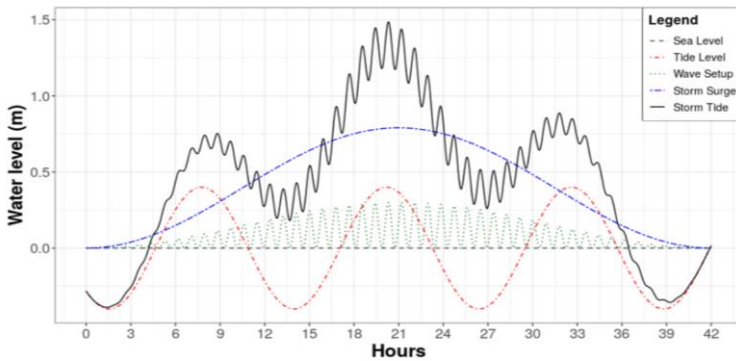
The nearshore ESL scenarios specified in Table 1 and exemplified in Figure 4 (and Annex 1) are used as a nearshore forcing boundary condition in the set-up of ANUGA. ANUGA is a 2D hydrodynamic model suitable for the simulation of flooding resulting from riverine peak flows and storm surges (Roberts, 2020). The fluid dynamics simulation is based on a finite-volume method for solving the shallow water wave equations, thus being based on continuity and simplified momentum equation. Being a 2D hydrodynamic model, ANUGA does not resolve vertical convection, waves breaking or 3D turbulence (i.e. vorticity), thus it cannot account for the swash component of wave runup. Wave direction is set to be oriented perpendicular to the coast. ANUGA is a 2D hydrodynamic model suitable for the simulation of flooding resulting from riverine peak flows and storm surges (ANUGA – Open source hydrodynamic/hydraulic modelling). The fluid dynamics simulation is based on a finite-volume method for solving the shallow water wave equations, thus being based on continuity and simplified momentum equation. Being a 2D hydrodynamic model, ANUGA does not resolve vertical convection, waves breaking or 3D turbulence (i.e. vorticity), thus it cannot account for the swash component of wave runup. Yet the model is arranged to account for the wave setup component, based on the range of values reported in Table 1 and trigonometric functions presented in Annex 1 (A1.3, A1.4). In our simulations, wave direction is set to be oriented perpendicular to the coast. We consider wave setup as a function of the intensity of the storm surge level; thus, the maximum wave setup level is designed to coincide with the timing of maximum storm tide level, following the assumption of worst case scenario.

These hypothetical events are designed assuming trigonometric functional forms describing the oscillation of water level due to the different components defining ESL (Boon, 2011; Familkhalili et al., 2020; Fuhrmann et al., 2019).

At the local scale, hydrodynamic models represent an efficient compromise between hydrostatic and hydraulic models, being able to perform realistic simulations of inundation phenomena and to obtain detailed information about the hazard features, while requiring a relatively fast setup and reasonable computational effort. In this study we use ANUGA, a 2D hydrodynamic model originally developed to simulate tsunami events, which is also suitable for the simulation of hydrologic phenomena such as riverine peak flows and storm surges (ANUGA – Open source hydrodynamic/hydraulic modelling). Being a 2D hydrodynamic model, ANUGA does not resolve vertical convection, waves breaking or 3D turbulence (e.g. vorticity), thus it does not account for the swash component of wave runup. The fluid dynamics in ANUGA is based on a finite-volume method for solving the shallow water wave equations, thus being based on continuity and simplified momentum equation. The model computes the total water level, the water depth, and the horizontal momentum on an irregular triangular grid based on the provided forcing conditions specified in Table 1 for the ESL scenario RP 10. The individual contribution of storm, tide and wave setup is shown separately by coloured dashed lines, and summed up to generate the black continuous line representing the TWL: the storm surge rises the water level up by 0.60 m, high tide contribution grows from 0.40 m to 0.45 m,

411 and wave setup near the shore ranges from 0.22 m to 0.65 m. At the peak of the event, these conditions produce  
412 a maximum TWL of 1.49 m.

413 ANUGA includes also an operator module that simulates the removal of sand associated with over topping  
414 of a sand dune by sea waves, which is applied to explore scenarios where a sand dune barrier provides  
415 protection for the land behind. The operator simulates the erosion, collapse, fluidisation and removal of sand  
416 from the dune system (Kain et al. 2020); the dune erosion mechanism relies on a relationship based on  
417 Froehlich (2002). This option is enabled only in the undefended scenario for Cesenatico, where non-reinforced  
418 sand dunes are prone to erosion.



419  
420 **Figure 44.** Total Water Level (black) as a sum of tide (red), storm surge (blue) and wave setup (green) for ESL  
421 scenario 1 in 10 years. Additional figures for all RPs are found in Annex 1.

422 In our application, we estimate the TWL on the coastland at every timestep as the sum of extreme values for  
423 storm surge level (SS), wave setup (Ws), and max tide (Tmax), as shown in figure 4. Storm surge peak is set to  
424 coincide with the tidal peak at the mid of the event, thus producing a maximum TWL value. As considered,  
425 our approach is precautionary as it provides worst case scenario ESL values. The components of TWL are  
426 obtained from existing probabilistic analysis of extreme events conducted on the regional coast (Perini et al.,  
427 2016, 2017) and later adopted by the Regional Environmental Agency to define the official coastal flood hazard  
428 zones (ARPA Emilia Romagna, 2019). The probability of occurrence for ESL scenarios is expressed in terms of  
429 return period (RP), which is the estimated average time interval between events of similar intensity,  
430 accounting for all variables combined. The maximum tidal excursion is 0.8-0.9 m, while wave setup near the  
431 shore can range from 0.22 to 0.65 m. For RP 250, TWL hits 2.5 meters as all components reach their most  
432 extreme values. Additional details are wave period (Wp, in seconds) and event duration (Time, in hours),  
433 required for the hydrodynamic simulation of coastal flooding events and the determination of the maximum  
434 extent of inland water propagation. Both variables are obtained from existing analysis of historical ESL events  
435 records matched with the probabilistic distribution of RP scenarios (Armaroli et al., 2012; Armaroli and Duo,  
436 2018). In our scenarios, wave direction is set to be oriented perpendicular to the coast. Table 1 summarizes the  
437 ESL components according to the four probability scenarios identified from local historical records (Perini et  
438 al. 2017). The output of the simulation consists of maps representing flood extent, water depth and momentum  
439 at every time step (1 second), projected on the high-resolution DTM grid.

440 For each scenario, the model ANUGA can compute the TWL insisting on the coast, the resulting water depth  
441 of inundation, and the horizontal momentum on an unstructured triangular grid (mesh) representing the two

Field Code Changed

case study areas. The size of the triangles is variable within the mesh, thus allowing for a better representation in regions of particular interest, such as along the coastline, in urban areas, and inside the canals. Six different regions are used in each case study to define different triangular mesh resolution, varying from higher resolution areas of 16 m<sup>2</sup> for canals and coastal defence structures, to lower resolution of 900 m<sup>2</sup> for sea areas. The output of the simulation consists of maps representing flood extent, water depth and momentum at every time step (~1 second), projected on the high-resolution DTM grid (1 meter). Figure 6 presents the two case study areas and the respective resolutions for each region. The resulting irregular mesh counts with about 637 thousand triangles for the Cesenatico domain, and about 1,2 million triangles for the Rimini domain. The model includes an operator module that simulates the removal of sand associated with over-topping of a sand dune by sea waves. The operator simulates the erosion, collapse, fluidisation and removal of sand from the dune system (Kain et al., 2020). This option is enabled only in the undefended scenario for Cesenatico, where non-reinforced sand dunes are prone to erosion.

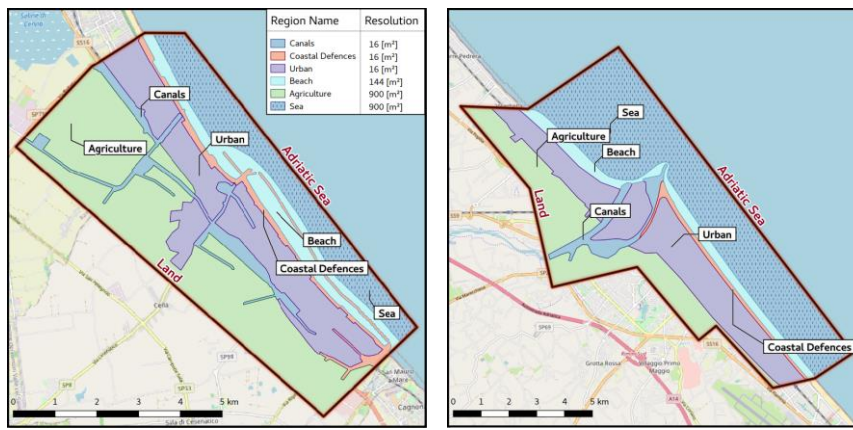


**Figure 5.** The definition of simulation domain for the cities of Cesenatico (on the left) and Rimini (on the right). The legend shows the mesh resolution specific to each region simulated by the model.

ANUCA takes into account the boundary conditions specified in Table 1 and dynamically shown in Figure 5 to simulate the flood dynamics within the domain, such as water flowing through canals and the flooding of land areas. For each return period scenario, a different idealized storm tide event is designed in order to match the maxima level of tide and surge (following the worst case scenario assumption, as previously mentioned). The idealized storm tide events are designed assuming trigonometric functional forms describing the oscillation of water level due to the different components defining ESL (CITATIONS2). Each component, then, has a different period and magnitude, to reflect specific contributions of each component. Regarding the wave component, since ANUCA is a 2D model that cannot simulate wave breaking and the swash component of wave runup, we simulate just the wave setup component using data obtained from the literature (CITATION2). The wave setup is a relevant component of the total water level by contributing to the flood dynamics due to the momentum of waves, particularly when directed inlands (CITATION2). We consider wave setup as a function of the intensity of the storm surge level, as shown in Figure 5. The maximum wave setup level is designed to coincide with the maximum storm tide level, following the assumption of worst-



case scenario, while wave direction is aligned with the storm surge direction, thus being perpendicular to the coastline.

### 3.9.3.8 Risk modelling and Expected Annual Damage

Direct damage to physical asset is estimated using a customary flood risk assessment approach originally developed for fluvial inundation, which is adapted to coastal flooding assuming that the dynamic of impact from long-setting floods depends on the same factors, namely: 1) hazard magnitude, and 2) type, size and value of exposed asset. Indirect economic losses due to secondary effects of damage (e.g. business interruption) are excluded from the computation. Hazard magnitude can be defined by a range of variables, but the most important predictors of damage are water depth and the extension of the flood event (Jongman et al., 2012a; Huizinga et al., 2017). ~~Land cover definitions and buildings footprints help to estimate the exposed capital including residential buildings, commercial and industrial activities, infrastructures, historical and natural sites.~~ The characterization of exposed asset is built from a variety of sources, starting from land use and buildings footprints obtained from the Regional Environmental Agencies geodatabases and the Open Street Map database (Open Street Map data for Nord-Est Italy, 2019). Additional indicators about buildings characteristics are obtained from the database of the 2011 Italian Census (15° censimento della popolazione e delle abitazioni, 2019), while mean construction and restoration costs per building types are obtained from cadastral estimates (CRESME, 2019). The asset representation is static, thus not accounting for changes in land use nor population density, while allowing for the direct comparison of hazard mitigation options' results. A depth-damage function ~~was previously~~ validated on empirical records (Amadio et al., 2019) ~~and then is~~ applied in order to translate each hazard scenario into an estimate of economic risk, measured as a share of total exposed value. The damage function applies only to residential and mixed-residential buildings, the area of which represents about 93% of total exposed footprints; other types (such as harbour infrastructures, industrial, commercial, historical monuments and natural sites) are excluded from risk computation. Abandoned or under-construction buildings are also excluded from the analysis. To avoid overcounting of marginally-affected buildings, we set two threshold conditions for damage calculation: flood extent must be greater than or equal to 10 m<sup>2</sup>, and maximum water depth must be greater than or equal to 10 cm. The damage/probability scenarios are combined together as Expected Annual Damage (EAD). EAD is the damage that would occur in any given year if damages from all flood probabilities were spread out evenly over time; mathematically, EAD is the integration of the flood risk density curve over all probabilities (Olsen et al., 2015), as in equation 1.

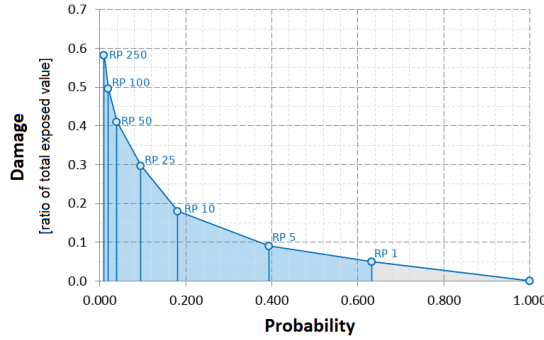
$$EAD = \int_0^1 D(p) dp \quad (1)$$

The integration of the curve can be solved either analytically or numerically, depending on the complexity of the damage function  $D(p)$ . Several different methods for numerical integration exist; we use an approach where EAD is the sum of the product of the fractions of exceedance probabilities by their corresponding damages (~~Figure 75~~). We calculate  $D(p)$ , which is the damage that occurs at the event with probability  $p$ , by using the depth-damage function for each hazard scenario. The exceedance probability of each event ( $p$ ) is calculated based on exponential function as shown in equation 2.

$$p = 1 - e^{\left(\frac{-1}{RP}\right)} \quad (2)$$

Events with a high probability of occurrence and low intensity (below RP 1 year) are not simulated, as they are assumed to not cause significant damage. This is consistent with the historical observations for the case study area, although this assumption could change with increasing MSL.

**Figure 665.** Schematic representation of the numerical integration of the damage function  $D(p)$  with respect to the exponential probability of the hazard events. Damage (Y axis) represents the ratio of damage to the total exposed value estimated up to the most extreme scenario (RP 250 years). Events with a probability of occurrence higher than once in a year are expected to not cause damage (grey area).



### 3.4.3.9 Cost-Benefit Analysis

A CBA should include a complete assessment of the impacts brought by the implementation of the hazard mitigation option, i.e. direct and indirect, tangible and intangible impacts (Bos and Zwaneveld, 2017). The project we are considering, however, has not been primarily designed for DRR purpose: instead, it is meant as an urban renovation project which aims to consolidate the touristic vocation of the area, to improve the quality of life and the urban environment (Comune di Rimini, 2018). This implies some large indirect effects on the whole area, most of which are not strictly related to disaster risk management and, overall, very difficult to estimate ex-ante. Our evaluation focuses only on the benefits that are measurable in terms of direct flood losses reduction. Regarding the implementation costs, the CBA accounts for the initial investment required for setting up the adaptation measure, and operational costs through time. According to the *Parco del Mare* project funding documentation (Comune di Rimini, 2019b, a, 2020, 2021a, b), the total cost of the project (to be completed during 2021) is 33.3 M Eur, corresponding to 5.55 M Eur per Km of length. No information is available about maintenance costs of the opera, but given the nature of the project (static defense with low structural fragility), we assume they will be rather small compared to the initial investment. Ordinary annual maintenance costs are accounted as 0.1% of the total cost of the project. The same costs are assumed for the hypothetical barrier in Cesenatico, resulting in an initial investment cost of 43.3 M. Costs and benefit occurring in the future periods need to be discounted, as people put higher value on the present (Rose et al., 2007). This is done by adjusting future costs and benefits using an annual discount rate ( $r$ ). We chose a variable rate of  $r = 3.5$  for the first 50 years and  $r = 3$  from 2050 onward (Lowe, 2008). A sensitivity analysis of discount rate is included in Annex 42. The three main decision criteria used in CBA for project evaluation are the Net Present Value (NPV), the Benefit/Cost Ratio (BCR) and the payback period. The NPV is the sum of Expected Annual Benefits ( $B$ ) up to the end of the time horizon, discounted, minus the total costs for the implementation of the defense measure, which takes into account initial investment plus discounted annual maintenance costs ( $C$ ). In other words, the NPV of a project equals the present value of the net benefits ( $NB_i = B_i - C_i$ ) over a period of time (Boardman et al., 2018), as in equation (3):

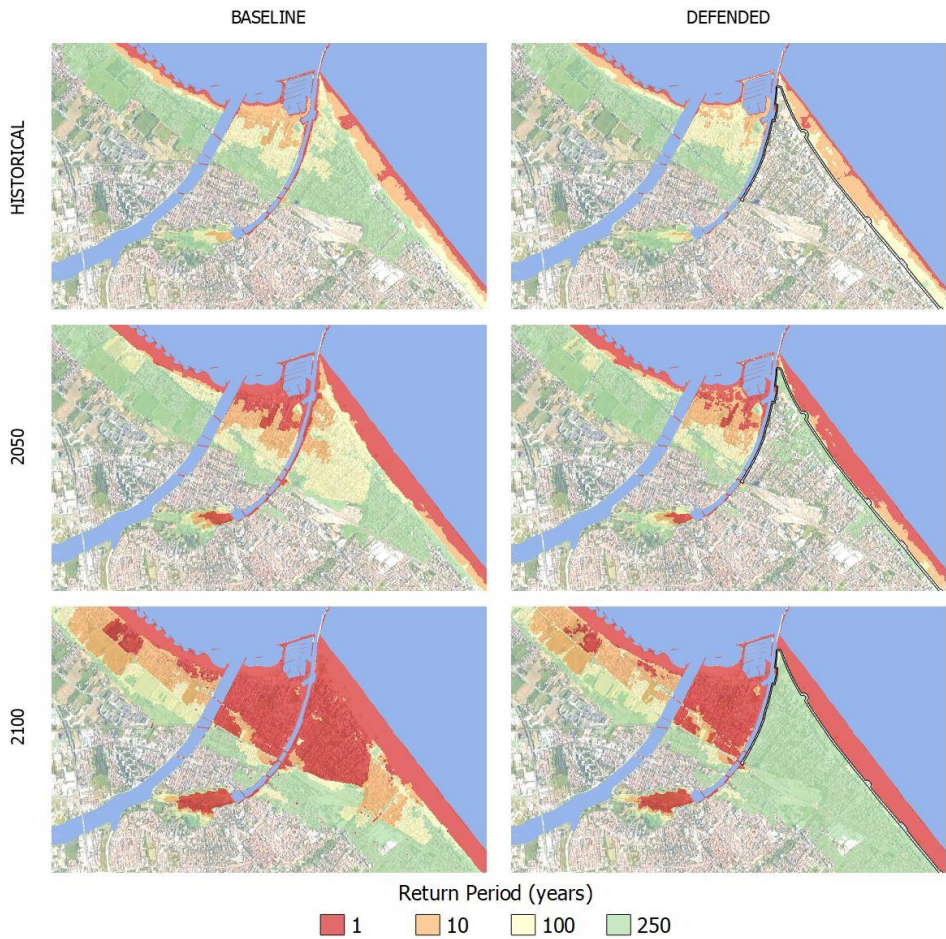
$$NPV = PV(B) - PV(C) = \sum_{t=0}^n \frac{NB_t}{(1+r)^t} \quad (3)$$

Positive NPV means that the project is economically profitable. The BCR is instead the ratio between the benefits and the costs; a BCR larger than 1 means that the benefits of the project exceed the costs on the long term and the project is considered profitable. The payback period is the number of years required for the discounted benefits to equal the total costs.

539 4. Results

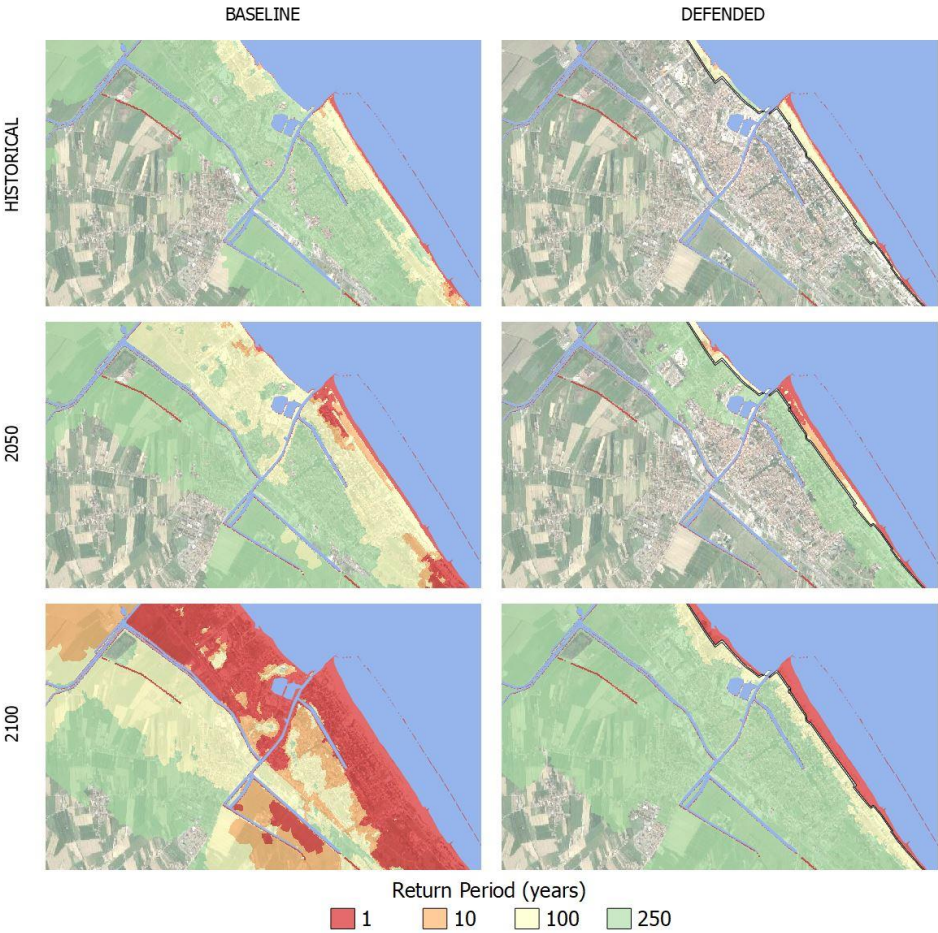
540 4.1 Inundation scenarios

541 Once the setup is completed, the hydrodynamic model performs relatively fast: each simulation is carried at  
542 half speed compared to real time, requiring about 24 hours to simulate a 12 h event. Parallel simulations for  
543 the same area can run on a multicore processor, improving the efficiency of the process. The output of the  
544 hydrodynamic model consists of a set of inundation simulations that include several hazard intensity variables  
545 in relation to flood extent: water depth, flow velocity, and duration of submersion. ESL scenarios are then  
546 summarized into static maps, each one representing the maximum value reached by hazard intensity variables  
547 during the simulated event at about 1 meter resolution. The flood extents corresponding to each RP scenario  
548 are shown for Rimini (Figure 86) and Cesenatico (Figure 97).



549  
550 **Figure 776.** Rimini, extent of land affected by flood according to frequency of occurrence of ESL event up to  
551 2100 for the baseline [left] and the defended scenario [right]. Basemap © Google Maps 2020.

552 In Rimini, the *Parco del Mare* barrier produces benefits in terms of avoided damage-flooding in the south-  
 553 eastern part of the town (high-density area) for ESL events with a return period of 100 years or less. The north-  
 554 western part and the marina are outside of the defended area; these areas are therefore subject to a similar  
 555 amount of flooding across scenarios. In all the simulations, the buildings located behind the marina are the  
 556 firsts to be flooded. In fact, the new and the old port channels located on both sides of the marina represent a  
 557 hazard hotspot: as shown in the maps, the failure of the eastern channel, which has a relatively low elevation,  
 558 is likely to cause the water to flood the eastern part of the town, even during inundation events that would  
 559 not surpass the beach. In the defended scenarios, where both the coastal and the canal barriers are enabled,  
 560 the flood extent in the south-eastern urban area becomes almost zero for ESL events with a probability of once  
 561 in 100 years, even when accounting for SLR up to 2100. Under the most exceptional ESL conditions (RP 250 in  
 562 2100), the barrier is overtopped, generating a flood extent similar to the baseline scenario for the same  
 563 occurrence probability.



564  
 565 **Figure 887.** Cesenatico, extent of land affected by flood according to frequency of occurrence of ESL event up to 2100 for the baseline [left] and the defended scenario [right]. Basemap © Google Maps 2020.  
 566



In Cesenatico, a barrier designed similarly to *Parco del Mare* could provide significant reduction of flood extents under most hazard scenarios. Its effectiveness would be greater than in Rimini thanks to the complementary movable barrier system in use, which seals the port channel allowing to wall off the whole coastal perimeter, reducing the chance of water ingress in the urban area. In contrast, the erodible winter dune in the baseline defense scenario can only hold the heavy sea for shorter, less intense ESL events (RP 1 – 10 years), and becomes ineffective with more exceptional, long-lasting events; from 2050 on, the winter dune could be surmounted and dismantled by sea waves even during frequent-non-exceptional events (RP 1 year).

#### 4.2 Expected Annual Damage

The Expected Annual Damage is calculated as a function of maximum exposed value and water depth. In Rimini, the EAD grows from around 650 thousand Eur under historical conditions to 2.8 million Eur in 2050 and more than 32.3 million Eur in 2100. Under less severe ESL scenarios (RP below 100 years), the risk remains mostly confined around the marina, which is located outside the defended area, producing an expected damage below 10 thousand Eur. Under more extreme ESL scenarios, the benefits of the *Parco del Mare* project protecting the southern part of Rimini become more evident, avoiding about 65% of the expected damages in the defended scenarios compared to the undefended ones. The damage avoided in the defended scenarios grow almost linearly with the increase of the baseline EAD under future projections of sea level rise: under the defended scenario, the EAD is reduced on average by 45% in comparison with the undefended scenario (Figure 98, left). The project produces benefit up to scenario RP 250 years in 2100, where a projected TWL of 3.5 meters would cause the overtopping of the barrier, reducing the benefits to almost zero (Figure 89, right).

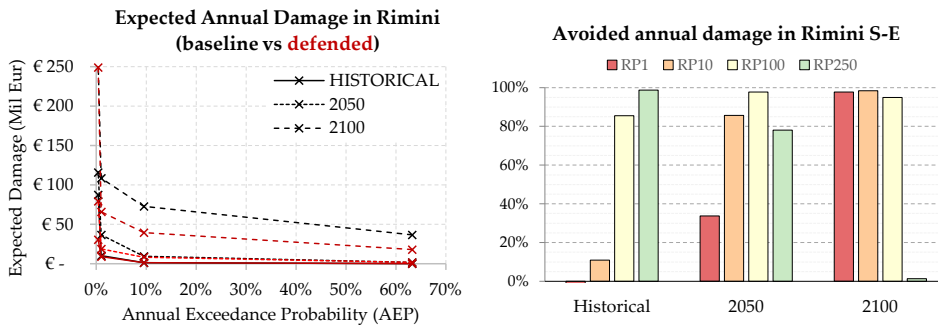


**Figure 98.** Rimini: Expected Annual Damage (EAD) according to undefended scenario up to 2100, all town considered [left]; EAD reduction in the south-eastern part of the town thanks to hazard mitigation offered by the coastal barrier [right].

In Cesenatico, the average EAD for the undefended scenario grows from around 270 thousand Eur under historical conditions, to 1.7 million Eur in 2050 and almost 26 million Eur in 2100. In our simulations, the designed defence structure (a static barrier with height of 2.8 m along 7.8 km of coast) is able to avoid most of the damage inflicted to residential buildings (Figure 119, left). The measure becomes less efficient for the most extreme scenarios in 2050 and 2100, when the increase in TWL causes the surmounting of the barrier (Figure 910, right). This assessment does not account for the impacts over those beach resorts and bathing facilities which are located along the barrier or between the barrier and the sea, and thus are equally exposed in both the baseline and the defended scenario; they would likely represent an additional 7-25% of the baseline damage.



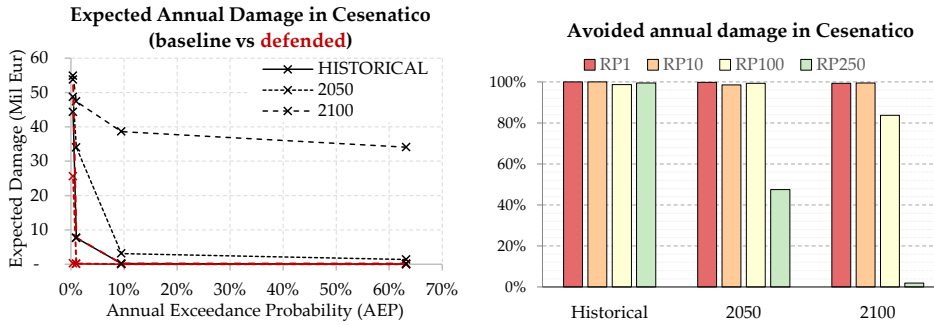


**Figure 10109.** Cesenatico: Expected Annual Damage (EAD) according to undefended scenario up to 2100 [left]; EAD reduction thanks to hazard mitigation offered by the coastal barrier [right].

#### 4.3 Cost-Benefit Analysis

The estimates of avoided direct flood impacts are accounted in a DRR-oriented CBA to evaluate the feasibility of mitigation measures in terms of NPV, BCR and payback period for the two time-horizons (2021-2050: 30 years; and 2021-2100: 80 years). The assessment does not measure the indirect benefits brought in terms of urban renovation, which are the primary focus of the *Parco del Mare* project, measuring, instead, only the direct benefits in terms of direct flood damage reduction. In [Figure 1210](#), the Expected Annual Benefits (EAB) brought by defence measures grow at faster rate approaching 2100 in both sites, because of the larger expected damages from increasing floods severity from more intense, less frequent flood events. The cost of defence implementation is repaid by avoided damage after about 40 years in Cesenatico and after 90 years in Rimini. At 2100, the BCR is 0.9 for Rimini and 1.8 for Cesenatico. These results clearly indicate an overall profitability of the defence structure implementation over the long term for Cesenatico. For the case of the municipality of Rimini, further investigation is required in order to account for the non-DRR benefits of the seafront renovation project. For instance, the potential reduction in indirect losses in terms of capital and labour productivity due to less frequent and less intense flooding events, and the potential increase in tourism and well-being of citizens due to renewed urban landscape, are factors that could be accounted for in a holistic CBA analysis and would likely return a shorter payback period.

**Table 2.** Summary of CBA for planned or designed seaside defence project in Rimini (all town and south section only) and Cesenatico (all town and center only) over a time horizon of 30 and 80 years (2021 to 2050 and 2021 to 2100).

Metrics	Rimini				Cesenatico			
	All town		South only		All town		Center only	
	2050	2100	2050	2100	2050	2100	2050	2100
Baseline EAD [M EUR]	2.8	32	0.5	14.6	1.7	25.9	0.5	12.4
Defended EAD [M EUR]	2.4	17	0.1	0.9	0.1	0.4	0.1	0.4
Expected Annual Benefits [M EUR]	0.3	15	0.4	13.7	1.6	25.5	0.4	11.9
Sum of EAB (discounted) [M EUR]	5.6	30	4.1	27.8	12.0	79.4	4.7	28.6
Sum of EAC (discounted) [M EUR]	33.8	34.0	33.8	34.0	43.8	44.3	15.8	16.0
Net Present Value [M EUR]	-28.3	-4.0	-29.8	-6.3	-31.8	35.1	-11.24	12.6
Benefit-Cost ratio [-]	0.16	0.88	0.12	0.81	0.28	1.79	0.30	1.79

In order to better understand the potential benefits of the mitigation measures over different areas of the two municipalities, we compare the results in terms of CBR over a selection of exposed records corresponding to the town higher-density area (i.e. Cesenatico historical center). Table 2 summarizes the metrics of the

assessment for different area extent selections. CBA results do not differ much when considering comparing the CBA over different areas extents. In Cesenatico benefits grow proportionally to costs, so that the payback time does not change when considering a section of the town or the whole coastal perimeter.

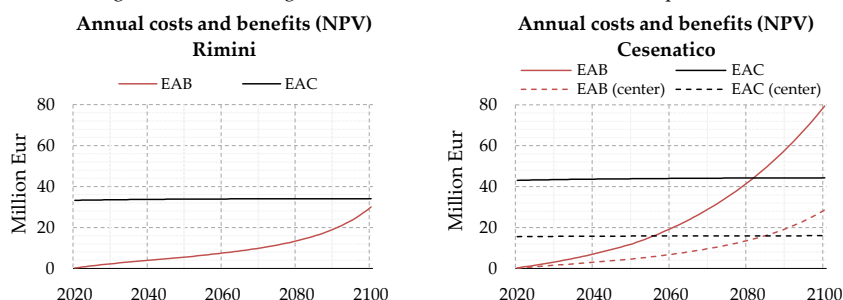


Figure 11. Cumulated flood defence costs and expected benefits at Net Present Value for Rimini (left) and Cesenatico (right).

## 5. Conclusion

In this study we addressed risk scenarios from coastal inundation risk scenarios over two coastal towns located along the North Adriatic coastal plain of Italy. This area which is projected to become increasingly exposed to ESL events due to changes in MSL induced by SLR and local subsidence phenomena. Both locations are expected to suffer increasing economic losses from these events, unless effective coastal adaptation measures are put in place. In order to understand the upcoming impacts and the potential benefits of designed coastal projects, we produced flood hazard maps estimating maximum flood extent and water depth using a high-resolution hydrodynamic model able to replicate the physics of the inundation process. First we designed probabilistic ESL scenarios based on local historical observations; then, we projected these scenarios to 2050 and 2100, accounting for the combined effect of SLR and subsidence rates on the MSL. By using a high-resolution hydrodynamic model, we produced flood hazard maps associated with each ESL scenario under both the baseline and the "defended" hypothesis. The defended scenarios accounts for the effect of a coastal barriers based on the design of Parco del Mare, an urban renovation project under construction in Rimini. The same type of defence structure is envisaged along the coastal perimeter of the nearby town of Cesenatico. The hazard maps were fed to a locally-calibrated damage model in order to calculate the expected annual damage for both baseline and defended scenarios.

We run a CBA comparing the baseline and the defended scenario expected damage in terms of flood losses over residential buildings, which represent the largest share of exposed buildings' footprints (93%). The defended scenario accounts for the effect of a coastal barriers based on the design of Parco del Mare, an urban renovation project under construction in Rimini. The same type of defence structure is envisaged along the coastal perimeter of the nearby town of Cesenatico. First, we characterised reference ESL events in terms of frequency and intensity based on local historical observations; then, we projected ESL scenarios to 2050 and 2100, accounting for the combined effect of eustatic SLR and subsidence rates on the TWL, as obtained from existing local studies. We produced flood hazard maps estimating maximum flood extent and water depth using a high-resolution hydrodynamic model able to replicate the physics of the inundation process. The hazard maps were fed to a locally-calibrated damage model in order to calculate the expected annual damage for both baseline and defended scenarios. An increase in damage is expected for both urban areas from 2021 to 2100: in Cesenatico the EAD grows by a factor 96, in Rimini by a factor 49.

659 The results ~~obtained from the CBA on both locations show show growing that~~ profitability of present project  
 660 investment ~~grows~~ over time ~~in both locations, associated due to with the the~~ increase of ~~expected~~ damage  
 661 triggered by intense ESL events: the EAD under the baseline hypothesis is expected to increase by 3.5-fold in  
 662 2050, up to 10-fold in 2100. The benefits brought by the coastal defence project become much larger in the  
 663 second half of the century: the EAB grows 6.1-fold in Rimini, 6.5-fold in Cesenatico, from 2050 to 2100. Avoided  
 664 losses are expected to match the project implementation costs after about 40 years in Cesenatico and 90 years  
 665 in Rimini. Benefits are found to increase proportionally to costs; the payback period in Cesenatico is the same  
 666 considering either an investment on the protection of the whole town or only part of it. Further assessments  
 667 of these renovation projects should look to measure the indirect and spill-over effects over the local economy  
 668 brought by the project, possibly accounting also for the intangible benefits and scenarios of exposure change.  
 669 The results are calculated in relation to emission scenario RCP 4.5; compared to RCP 8.5 at 2050, the difference  
 670 in SLR contribution is negligible (~0.05 m), while at 2100, the difference between the two emission scenarios is  
 671 larger (around 0.2 m), thus additional scenario analysis is suggested ~~to better address risk by the end of the~~  
 672 ~~century in future research.~~

#### 673 Data availability

674 Mattia Amadio, & Arthur H. Essenfelder: (2021). Coastal flood inundation scenarios over Cesenatico and  
 675 Rimini: hazard and risk for Business as Usual and Defended options [Data set]. Hosted by Zenodo:  
 676 <https://zenodo.org/record/4783443>

#### 677 Authors contribution

678 MA, AHE and SB conceptualized the study and designed the experiments. AHE carried out the coastal hazard  
 679 modelling. SR advised the model setup and calculation. SB and PM provided required data and expertise  
 680 about the case study areas. MA performed the economic risk modelling and wrote the manuscript. SM  
 681 supported the CBA calculations. JM and SB managed the funding acquisition and project supervision. All co-  
 682 authors have reviewed the manuscript.

#### 683 Acknowledgment

684 The research leading to this paper received funding through the projects CLARA (EU's Horizon 2020 research  
 685 and innovation programme under grant agreement 730482), SAFERPLACES (Climate-KIC innovation  
 686 partnership) and EUCP – European Climate Prediction system under grant agreement 776613. We want to  
 687 thank Luisa Perini for her kind support.

#### 688 References

- 689 Amadio, M., Scorzini, A. R., Carisi, F., Essenfelder, A. H., Domeneghetti, A., Mysiak, J., and Castellarin, A.:  
 690 Testing empirical and synthetic flood damage models: the case of Italy, Nat. Hazards Earth Syst. Sci., 19,  
 691 661–678, <https://doi.org/10.5194/nhess-19-661-2019>, 2019.
- 692 Anderson, T. R., Fletcher, C. H., Barbee, M. M., Romine, B. M., Lemmo, S., and Delevalux, J. M. S. M. S.:  
 693 Modeling multiple sea level rise stresses reveals up to twice the land at risk compared to strictly passive  
 694 flooding methods, Sci. Rep., 8, 14484, <https://doi.org/10.1038/s41598-018-32658-x>, 2018.
- 695 Annunziato, A. and Probst, P.: Continuous Harmonics Analysis of Sea Level Measurements: Description of a  
 696 new method to determine sea level measurement tidal component, <https://doi.org/10.2788/4295>, 2016.
- 697 Antonioli, F., Anzidei, M., Amorosi, A., Lo Presti, V., Mastronuzzi, G., Deiana, G., De Falco, G., Fontana, A.,

**Commented [MA2]:** check your reference lists, because it contains incomplete information for several items, which would prevent readers accessing them (e.g. publications by "Comune di Rimini", CRESME, the ANUGA manual ...)

**Commented [MA3R2]:** Access urls have been provided when DOI is not available; Copernicus style format has been applied.

Fontolan, G., Lisco, S., Marsico, A., Moretti, M., Orrù, P. E., Sannino, G. M., Serpelloni, E., and Vecchio, A.: Sea-level rise and potential drowning of the Italian coastal plains: Flooding risk scenarios for 2100, *Quat. Sci. Rev.*, 158, 29–43, <https://doi.org/10.1016/j.quascirev.2016.12.021>, 2017.

Armaroli, C. and Duo, E.: Validation of the coastal storm risk assessment framework along the Emilia-Romagna coast, *Coast. Eng.*, 134, 159–167, <https://doi.org/10.1016/j.coastaleng.2017.08.014>, 2018.

Armaroli, C., Ciavola, P., Perini, L., Calabrese, L., Lorito, S., Valentini, A., and Masina, M.: Critical storm thresholds for significant morphological changes and damage along the Emilia-Romagna coastline, Italy, 143–144, 34–51, <https://doi.org/10.1016/j.geomorph.2011.09.006>, 2012.

ARPA Emilia-Romagna: Relazione Tecnica - Mappe della pericolosità e del rischio di alluvioni in ambito costiero, distretto Appennino Settentrionale, <https://ambiente.regione.emilia-romagna.it/it/suolo-bacino/sezioni/piano-di-gestione-del-rischio-alluvioni/piano-gestione-del-rischio-alluvioni/documenti-1/relazioni-tecniche-mappe/relazione-tecnica-mappe-della-pericolosita2019-e-del-rischio-di-alluvioni->, 2019.

Barnard, P. L., Erikson, L. H., Foxgrover, A. C., Hart, J. A. F., Limber, P., O'Neill, A. C., van Ormondt, M., Vitousek, S., Wood, N., Hayden, M. K., and Jones, J. M.: Dynamic flood modeling essential to assess the coastal impacts of climate change, *Sci. Rep.*, 9, 1–13, <https://doi.org/10.1038/s41598-019-40742-z>, 2019.

Bates, P. D., Dawson, R. J., Hall, J. W., Horritt, M. S., Nicholls, R. J., Wicks, J., and Ali Mohamed Hassan, M. A.: Simplified two-dimensional numerical modelling of coastal flooding and example applications, *Coast. Eng.*, 52, 793–810, <https://doi.org/10.1016/j.coastaleng.2005.06.001>, 2005.

Boardman, A. E., Greenberg, D. H., Vining, A. R., and Weimer, D. L.: *Cost-Benefit Analysis*, Cambridge University Press, <https://doi.org/10.1017/9781108235594>, 2018.

Bonaduce, A., Pinardi, N., Oddo, P., Spada, G., and Larnicol, G.: Sea-level variability in the Mediterranean Sea from altimetry and tide gauges, *Clim. Dyn.*, 47, 2851–2866, <https://doi.org/10.1007/s00382-016-3001-2>, 2016.

Boon, J. D.: *Secrets of the Tide*, Elsevier, 1–210 pp., <https://doi.org/10.1016/C2013-0-18114-7>, 2011.

Bos, F. and Zwaneveld, P.: Cost-Benefit Analysis for Flood Risk Management and Water Governance in the Netherlands: An Overview of One Century, *SSRN Electron. J.*, <https://doi.org/10.2139/ssrn.3023983>, 2017.

Bouwer, L. M.: Have disaster losses increased due to anthropogenic climate change?, *Bull. Am. Meteorol. Soc.*, <https://doi.org/10.1175/2010BAMS3092.1>, 2011.

Breilh, J. F., Chaumillon, E., Bertin, X., and Gravelle, M.: Assessment of static flood modeling techniques: Application to contrasting marshes flooded during Xynthia (western France), *Nat. Hazards Earth Syst. Sci.*, 13, 1595–1612, <https://doi.org/10.5194/nhess-13-1595-2013>, 2013.

Carbognin, L., Teatini, P., and Tosi, L.: The impact of relative sea level rise on the Northern Adriatic Sea coast, Italy, in: *WIT Transactions on Ecology and the Environment*, 137–148, <https://doi.org/10.2495/RAV090121>, 2009.

Carbognin, L., Teatini, P., Tomasin, A., and Tosi, L.: Global change and relative sea level rise at Venice: What impact in term of flooding, *Clim. Dyn.*, 35, 1055–1063, <https://doi.org/10.1007/s00382-009-0617-5>, 2010.

Carminati, E. and Martinelli, G.: Subsidence rates in the Po Plain, northern Italy: the relative impact of natural and anthropogenic causation, *Eng. Geol.*, 66, 241–255, [https://doi.org/10.1016/S0013-7952\(02\)00031-5](https://doi.org/10.1016/S0013-7952(02)00031-5), 2002.

Church, J. A. and White, N. J.: Sea-Level Rise from the Late 19th to the Early 21st Century, *Surv. Geophys.*, 32, 585–602, <https://doi.org/10.1007/s10712-011-9119-1>, 2011.

Ciavola, P. and Coco, G. (Eds.): *Coastal storms: processes and impacts*, Wiley-Blackwell, 266 pp., 2017.

Comune di Rimini: Parco del Mare Sud - Strategia per la rigenerazione urbana, <https://bit.ly/3kwNoB1>, 2018.

Comune di Rimini: Deliberazione originale di giunta comunale N. 118 del 02/05/2019, [https://www.comune.rimini.it/sites/default/files/2021-06/dlg\\_00118\\_02-05-2019.pdf](https://www.comune.rimini.it/sites/default/files/2021-06/dlg_00118_02-05-2019.pdf), 2019a.

Comune di Rimini: Deliberazione originale di giunta comunale N. 99 del 11/04/2019, [https://www.comune.rimini.it/sites/default/files/2021-06/dlg\\_00099\\_11-04-2019\\_0.pdf](https://www.comune.rimini.it/sites/default/files/2021-06/dlg_00099_11-04-2019_0.pdf), 2019b.

Comune di Rimini: Deliberazione originale di giunta comunale N. 128 del 26/05/2020,  
[https://www.comune.rimini.it/sites/default/files/2021-06/dlg\\_00128\\_26-05-2020.pdf](https://www.comune.rimini.it/sites/default/files/2021-06/dlg_00128_26-05-2020.pdf), 2020.

Comune di Rimini: Deliberazione originale di giunta comunale N. 19 del 19/01/2021,  
[https://www.comune.rimini.it/sites/default/files/2021-06/dlg\\_00019\\_19-01-2021.pdf](https://www.comune.rimini.it/sites/default/files/2021-06/dlg_00019_19-01-2021.pdf), 2021a.

Comune di Rimini: Deliberazione originale di giunta comunale N. 20 del 19/01/2021,  
[https://www.comune.rimini.it/sites/default/files/2021-06/dlg\\_00020\\_19-01-2021.pdf](https://www.comune.rimini.it/sites/default/files/2021-06/dlg_00020_19-01-2021.pdf), 2021b.

CRESME: I costi di costruzione in edilizia residenziale, industriale per uffici ed alberghiera,  
<http://cresme.cineas.it>, 2019.

Dottori, F., Martina, M. L. V., and Figueiredo, R.: A methodology for flood susceptibility and vulnerability  
 analysis in complex flood scenarios, *J. Flood Risk Manag.*, 11, S632–S645, <https://doi.org/10.1111/jfr3.12234>,  
 2018.

Famikhali, R., Talke, S. A., and Jay, D. A.: Tide-Storm Surge Interactions in Highly Altered Estuaries: How  
 Channel Deepening Increases Surge Vulnerability, *J. Geophys. Res. Ocean.*, 125, e2019JC015286,  
<https://doi.org/10.1029/2019JC015286>, 2020.

Fuhrmann, C. M., Wood, K. M., and Rodgers, J. C.: Assessment of storm surge and structural damage on San  
 Salvador Island, Bahamas, associated with Hurricane Joaquin (2015), *Nat. Hazards*, 99, 913–930,  
<https://doi.org/10.1007/s11069-019-03782-2>, 2019.

Gambolati, G., Giunta, G., Putti, M., Teatini, P., Tomasi, L., Betti, I., and Morelli, M.: Coastal Evolution of the  
 Upper Adriatic Sea due to Sea Level Rise and Natural and Anthropogenic Land Subsidence, 1–34,  
<https://doi.org/10.1007/978-94-011-5147-4>, 1998.

Garnier, E., Ciavola, P., Spencer, T., Ferreira, O., Armaroli, C., and McIvor, A.: Historical analysis of storm  
 events: Case studies in France, England, Portugal and Italy, *Coast. Eng.*, 134, 10–23,  
<https://doi.org/10.1016/j.coastaleng.2017.06.014>, 2018.

Hallegatte, S., Green, C., Nicholls, R. J., and Corfee-Morlot, J.: Future flood losses in major coastal cities, *Nat.*  
*Clim. Chang.*, <https://doi.org/10.1038/nclimate1979>, 2013.

Hinkel, J., Nicholls, R. J., Vafeidis, A. T., Tol, R. S. J., and Avagianou, T.: Assessing risk of and adaptation to  
 sea-level rise in the European Union: An application of DIVA, *Mitig. Adapt. Strateg. Glob. Chang.*,  
<https://doi.org/10.1007/s11027-010-9237-y>, 2010.

Hinkel, J., Lincke, D., Vafeidis, A. T., Perrette, M., Nicholls, R. J., Tol, R. S. J., Marzeion, B., Fettweis, X.,  
 Ionescu, C., and Levermann, A.: Coastal flood damage and adaptation costs under 21st century sea-level  
 rise, *Proc. Natl. Acad. Sci.*, 111, 3292–3297, <https://doi.org/10.1073/pnas.1222469111>, 2014.

Huizinga, J., Moel, H. De, and Szwedczyk, W.: Global flood depth-damage functions : Methodology and the  
 Database with Guidelines, 1–108 pp., <https://doi.org/10.2760/16510>, 2017.

Idier, D., Bertin, X., Thompson, P., and Pickering, M. D.: Interactions Between Mean Sea Level, Tide, Surge,  
 Waves and Flooding: Mechanisms and Contributions to Sea Level Variations at the Coast,  
<https://doi.org/10.1007/s10712-019-09549-5>, 1 November 2019.

ISPRA: Mare e ambiente costiero, Tematiche in Primo Piano - Annuario dei dati ambientali 2011, 259–322  
 pp., [https://www.isprambiente.gov.it/it/pubblicazioni/stato-dellambiente/tematiche-in-primo-piano-](https://www.isprambiente.gov.it/it/pubblicazioni/stato-dellambiente/tematiche-in-primo-piano-annuario-dei-dati-ambientali-2011)  
[annuario-dei-dati-ambientali-2011](https://www.isprambiente.gov.it/it/pubblicazioni/stato-dellambiente/tematiche-in-primo-piano-annuario-dei-dati-ambientali-2011), 2012.

Rete Mareografica Nazionale:  
[https://www.mareografico.it/?session=052731884245M826885M79QA&syslng=ita&sysmen=-1&sysind=-](https://www.mareografico.it/?session=052731884245M826885M79QA&syslng=ita&sysmen=-1&sysind=-1&syssub=-1&sysfnt=0&code=STAZ&idst=15)  
[1&syssub=-1&sysfnt=0&code=STAZ&idst=15](https://www.mareografico.it/?session=052731884245M826885M79QA&syslng=ita&sysmen=-1&sysind=-1&syssub=-1&sysfnt=0&code=STAZ&idst=15), last access: 19 October 2021.

15° censimento della popolazione e delle abitazioni: <http://dati-censimentopopolazione.istat.it>, last access: 1  
 April 2019.

Jongman, B., Kreibich, H., Apel, H., Barredo, J. I., Bates, P. D., Feyen, L., Gericke, A., Neal, J., Aerts, J. C. J. H.,  
 and Ward, P. J.: Comparative flood damage model assessment: towards a European approach, *Nat. Hazards*  
*Earth Syst. Sci.*, 12, 3733–3752, 2012a.

Jongman, B., Ward, P. J., and Aerts, J. C. J. H.: Global exposure to river and coastal flooding: Long term



trends and changes, *Glob. Environ. Chang.*, <https://doi.org/10.1016/j.gloenvcha.2012.07.004>, 2012b.

Jonkman, S. N., Brinkhuis-Jak, M., and Kok, M.: Cost benefit analysis and flood damage mitigation in the Netherlands, 49, 95–111, 2004.

Kain, C. L., Lewarn, B., Rigby, E. H., and Mazengarb, C.: Tsunami Inundation and Maritime Hazard Modelling for a Maximum Credible Tsunami Scenario in Southeast Tasmania, Australia, *Pure Appl. Geophys.*, 177, 1549–1568, <https://doi.org/10.1007/s00024-019-02384-0>, 2020.

Kemp, A. C., Horton, B. P., Donnelly, J. P., Mann, M. E., Vermeer, M., and Rahmstorf, S.: Climate related sea-level variations over the past two millennia, *Proc. Natl. Acad. Sci.*, 108, 11017–11022, <https://doi.org/10.1073/pnas.1015619108>, 2011.

Kind, J. M.: Economically efficient flood protection standards for the Netherlands, *J. Flood Risk Manag.*, 7, 103–117, <https://doi.org/10.1111/jfr3.12026>, 2014.

Kirezci, E., Young, I. R., Ranasinghe, R., Muis, S., Nicholls, R. J., Lincke, D., and Hinkel, J.: Projections of global-scale extreme sea levels and resulting episodic coastal flooding over the 21st Century, *Sci. Rep.*, 10, 11629, <https://doi.org/10.1038/s41598-020-67736-6>, 2020.

Kumbier, K., Carvalho, R. C., Vafeidis, A. T., and Woodroffe, C. D.: Comparing static and dynamic flood models in estuarine environments: a case study from south-east Australia, *Mar. Freshw. Res.*, 70, 781, <https://doi.org/10.1071/MF18239>, 2019.

Lambeck, K. and Purcell, A.: Sea-level change in the Mediterranean Sea since the LGM: model predictions for tectonically stable areas, *Quat. Sci. Rev.*, 24, 1969–1988, <https://doi.org/10.1016/j.quascirev.2004.06.025>, 2005.

Lambeck, K., Antonioli, F., Anzidei, M., Ferranti, L., Leoni, G., Scicchitano, G., and Silenzi, S.: Sea level change along the Italian coast during the Holocene and projections for the future, *Quat. Int.*, 232, 250–257, <https://doi.org/10.1016/j.quaint.2010.04.026>, 2011.

Lewis, M., Bates, P., Horsburgh, K., Neal, J., and Schumann, G.: A storm surge inundation model of the northern Bay of Bengal using publicly available data, *Q. J. R. Meteorol. Soc.*, 139, 358–369, <https://doi.org/10.1002/qj.2040>, 2013.

Li, M., Zhang, F., Barnes, S., and Wang, X.: Assessing storm surge impacts on coastal inundation due to climate change: case studies of Baltimore and Dorchester County in Maryland, *Nat. Hazards*, 103, 2561–2588, <https://doi.org/10.1007/s11069-020-04096-4>, 2020.

Lionello, P.: The climate of the Venetian and North Adriatic region: Variability, trends and future change, *Phys. Chem. Earth, Parts A/B/C*, 40–41, 1–8, <https://doi.org/10.1016/j.pce.2012.02.002>, 2012.

Lionello, P., Conte, D., Marzo, L., and Scarascia, L.: The contrasting effect of increasing mean sea level and decreasing storminess on the maximum water level during storms along the coast of the Mediterranean Sea in the mid 21st century, *Glob. Planet. Change*, 151, 80–91, <https://doi.org/10.1016/j.gloplacha.2016.06.012>, 2017.

Lionello, P., Barriopedro, D., Ferrarin, C., Nicholls, R., Orlic, M., Raichich, F., Reale, M., Umgiesser, G., Voudoukas, M., and Zanchettin, D.: Extremes floods of Venice: characteristics, dynamics, past and future evolution, *Nat. Hazards Earth Syst. Sci.*, 1–34, <https://doi.org/10.5194/nhess-2020-359>, 2020.

Lionello, P., Barriopedro, D., Ferrarin, C., Nicholls, R. J., Orlic, M., Raichich, F., Reale, M., Umgiesser, G., Voudoukas, M., and Zanchettin, D.: Extreme floods of Venice: Characteristics, dynamics, past and future evolution (review article), <https://doi.org/10.5194/nhess-21-2705-2021>, 1 September 2021.

Lowe, J.: Intergenerational wealth transfers and social discounting: Supplementary Green Book guidance, HM Treasury, London, 3–6, 2008.

Lowe, J., Gregory, J., and Flather, R.: Changes in the occurrence of storm surges around the United Kingdom under a future climate scenario using a dynamic storm surge model driven by the Hadley Centre climate models, *Clim. Dyn.*, 18, 179–188, 2001.

Marsico, A., Lisco, S., Lo Presti, V., Antonioli, F., Amorosi, A., Anzidei, M., Deiana, G., De Falco, G., Fontana, A., Fontolan, G., Moretti, M., Orrù, P. E., Serpelloni, E., Sannino, G., Vecchio, A., and Mastronuzzi, G.:

841 Flooding scenario for four Italian coastal plains using three relative sea level rise models, *J. Maps*, 13, 961–  
842 967, <https://doi.org/10.1080/17445647.2017.1415989>, 2017.

843 Masina, M., Lamberti, A., and Archetti, R.: Coastal flooding: A copula based approach for estimating the  
844 joint probability of water levels and waves, *Coast. Eng.*, 97, 37–52,  
845 <https://doi.org/10.1016/j.coastaleng.2014.12.010>, 2015.

846 McGranahan, G., Balk, D., and Anderson, B.: The rising tide: Assessing the risks of climate change and  
847 human settlements in low elevation coastal zones, *Environ. Urban.*,  
848 <https://doi.org/10.1177/0956247807076960>, 2007.

849 McInnes, K. L., Walsh, K. J. E., Hubbert, G. D., and Beer, T.: Impact of sea-level rise and storm surges in a  
850 coastal community, *Nat. Hazards*, 30, 187–207, <https://doi.org/10.1023/A:1026118417752>, 2003.

851 McInnes, K. L., O’Grady, J. G., and Hubbert, G. D.: Modelling sea level extremes from storm surges and  
852 wave setup for climate change assessments in Southeastern Australia, in: *Journal of Coastal Research*, 1005–  
853 1009, 2009.

854 Mechler, R.: Reviewing estimates of the economic efficiency of disaster risk management: opportunities and  
855 limitations of using risk-based cost–benefit analysis, *Nat. Hazards*, 81, 2121–2147,  
856 <https://doi.org/10.1007/s11069-016-2170-y>, 2016.

857 Melet, A., Almar, R., Hemer, M., Le Cozannet, G., Meyssignac, B., and Ruggiero, P.: Contribution of Wave  
858 Setup to Projected Coastal Sea Level Changes, *J. Geophys. Res. Ocean.*, 125, e2020JC016078,  
859 <https://doi.org/10.1029/2020JC016078>, 2020.

860 Meli, M., Olivieri, M., and Romagnoli, C.: Sea-Level Change along the Emilia-Romagna Coast from Tide  
861 Gauge and Satellite Altimetry, *Remote Sens.*, 13, 97, <https://doi.org/10.3390/rs13010097>, 2020.

862 Meyssignac, B. and Cazenave, A.: Sea level: A review of present-day and recent-past changes and variability,  
863 *J. Geodyn.*, 58, 96–109, <https://doi.org/10.1016/j.jog.2012.03.005>, 2012.

864 Mitchum, G. T., Nerem, R. S., Merrifield, M. A., and Gehrels, W. R.: Modern Sea-Level-Change Estimates, in:  
865 *Understanding Sea-Level Rise and Variability*, Wiley-Blackwell, Oxford, UK, UK, 122–142,  
866 <https://doi.org/10.1002/9781444323276.ch5>, 2010.

867 Muis, S., Güneralp, B., Jongman, B., Aerts, J. C. J. H., and Ward, P. J.: Flood risk and adaptation strategies  
868 under climate change and urban expansion: A probabilistic analysis using global data, *Sci. Total Environ.*,  
869 538, 445–457, <https://doi.org/10.1016/j.scitotenv.2015.08.068>, 2015.

870 Muis, S., Verlaan, M., Winsemius, H. C., Aerts, J. C. J. H., and Ward, P. J.: A global reanalysis of storm surges  
871 and extreme sea levels, *Nat. Commun.*, 7, 11969, <https://doi.org/10.1038/ncomms11969>, 2016.

872 Muis, S., Apecechea, M. I., Dullaart, J., de Lima Rego, J., Madsen, K. S., Su, J., Yan, K., and Verlaan, M.: A  
873 High-Resolution Global Dataset of Extreme Sea Levels, Tides, and Storm Surges, Including Future  
874 Projections, *Front. Mar. Sci.*, 7, 263, <https://doi.org/10.3389/fmars.2020.00263>, 2020.

875 Nicholls, R. J. and Cazenave, A.: Sea-Level Rise and Its Impact on Coastal Zones, *Science (80-. )*, 328, 1517–  
876 1520, <https://doi.org/10.1126/science.1185782>, 2010.

877 Olsen, A. S., Zhou, Q., Linde, J. J., and Arnbjerg-Nielsen, K.: Comparing methods of calculating expected  
878 annual damage in urban pluvial flood risk assessments, 7, 255–270, <https://doi.org/10.3390/w7010255>, 2015.

879 Open Street Map data for Nord-Est Italy: <http://download.geofabrik.de/europe/italy/nord-est.html>, last  
880 access: 1 April 2019.

881 Peltier, W. R.: Global glacial isostasy and the surface of the ice-age Earth: the ICE-5G model and GRACE,  
882 *Annu. Rev. Earth Planet. Sci.*, 32, 111–149, <https://doi.org/10.1146/annurev.earth.32.082503.144359>, 2004.

883 Peltier, W. R., Argus, D. F., and Drummond, R.: Space geodesy constrains ice age terminal deglaciation: The  
884 global ICE-6G\_C (VM5a) model, *J. Geophys. Res. Solid Earth*, 120, 450–487,  
885 <https://doi.org/10.1002/2014JB011176>, 2015.

886 Perini, L., Calabrese, L., Deserti, M., Valentini, A., Ciavola, P., and Armaroli, C.: Le mareggiate e gli impatti  
887 sulla costa in Emilia-Romagna 1946-2010, *Quaderni ARPA*,  
888 [https://www.researchgate.net/publication/290441941\\_Le\\_mareggiate\\_e\\_gli\\_impatti\\_sulla\\_costa\\_in\\_Emia](https://www.researchgate.net/publication/290441941_Le_mareggiate_e_gli_impatti_sulla_costa_in_Emia)

Romagna\_1946-2010, 2011.

Perini, L., Calabrese, L., Salerno, G., and Luciani, P.: Mapping of flood risk in Emilia-Romagna coastal areas, in: LXXXVI Congresso della Società Geologica Italiana, 501–502, <https://doi.org/http://dx.doi.org/10.13140/2.1.1703.7766>, 2012.

Perini, L., Calabrese, L., Lorito, S., and Luciani, P.: Il rischio da mareggiata in Emilia-Romagna: l'evento del 5-6 Febbraio 2015, *il Geologo*, 8–17 pp., [http://www.geologiemiliaromagna.it/wp-content/uploads/Art\\_Costa.pdf](http://www.geologiemiliaromagna.it/wp-content/uploads/Art_Costa.pdf), 2015.

Perini, L., Calabrese, L., Salerno, G., Ciavola, P., and Armaroli, C.: Evaluation of coastal vulnerability to flooding: comparison of two different methodologies adopted by the Emilia-Romagna region (Italy), *Nat. Hazards Earth Syst. Sci.*, 16, 181–194, <https://doi.org/10.5194/nhess-16-181-2016>, 2016.

Perini, L., Calabrese, L., Luciani, P., Olivieri, M., Galassi, G., and Spada, G.: Sea-level rise along the Emilia-Romagna coast (Northern Italy) in 2100: scenarios and impacts, *Nat. Hazards Earth Syst. Sci.*, 17, 2271–2287, <https://doi.org/10.5194/nhess-17-2271-2017>, 2017.

Polcari, M., Albano, M., Montuori, A., Bignami, C., Tolomei, C., Pezzo, G., Falcone, S., Piana, C. La, Doumaz, F., Salvi, S., and Stramondo, S.: InSAR monitoring of Italian coastline revealing natural and anthropogenic ground deformation phenomena and future perspectives, *Sustain.*, 10, 4–7, <https://doi.org/10.3390/su10093152>, 2018.

Pörtner, H. O., Roberts, D. C., Masson-Delmotte, V., Zhai, P., Tignor, M., Poloczanska, E., Mintenbeck, K., Alegría, A., Nicolai, M., Okem, A., Petzold, J., Rama, B., and Weyer, N. M.: IPCC Special Report on the Ocean and Cryosphere in a Changing Climate, IPCC, <https://www.ipcc.ch/srocc>, 2019.

Price, R.: Cost-effectiveness of disaster risk reduction and adaptation to climate change, 1–21, 2018.

Ramirez, J. A., Lichter, M., Coulthard, T. J., and Skinner, C.: Hyper-resolution mapping of regional storm surge and tide flooding: comparison of static and dynamic models, *Nat. Hazards*, 82, 571–590, <https://doi.org/10.1007/s11069-016-2198-z>, 2016.

Roberts, S.: ANUGA - Open source hydrodynamic/hydraulic modelling, <https://anuga.anu.edu.au>, 2020.

Roberts, S., Nielsen, O., Gray, D., and Sexton, J.: ANUGA User Manual, <https://doi.org/10.13140/RG.2.2.12401.99686>, 2015.

Scarascia, L. and Lionello, P.: Global and regional factors contributing to the past and future sea level rise in the Northern Adriatic Sea, *Glob. Planet. Change*, 106, 51–63, <https://doi.org/10.1016/j.gloplacha.2013.03.004>, 2013.

Seenath, A., Wilson, M., and Miller, K.: Hydrodynamic versus GIS modelling for coastal flood vulnerability assessment: Which is better for guiding coastal management?, *Ocean Coast. Manag.*, 120, 99–109, <https://doi.org/10.1016/j.ocecoaman.2015.11.019>, 2016.

Skinner, C. J., Coulthard, T. J., Parsons, D. R., Ramirez, J. A., Mullen, L., and Manson, S.: Simulating tidal and storm surge hydraulics with a simple 2D inertia based model, in the Humber Estuary, U.K, *Estuar. Coast. Shelf Sci.*, 155, 126–136, <https://doi.org/10.1016/j.ecss.2015.01.019>, 2015.

Smith, R. A. E., Bates, P. D., and Hayes, C.: Evaluation of a coastal flood inundation model using hard and soft data, *Environ. Model. Softw.*, 30, 35–46, <https://doi.org/10.1016/j.envsoft.2011.11.008>, 2012.

Solari, L., Del Soldato, M., Bianchini, S., Ciampalini, A., Ezquerro, P., Montalti, R., Raspini, F., and Moretti, S.: From ERS 1/2 to Sentinel-1: Subsidence Monitoring in Italy in the Last Two Decades, *Front. Earth Sci.*, 6, <https://doi.org/10.3389/feart.2018.00149>, 2018.

Stocker, T. F., Dahe, Q., Plattner, G.-K., Alexander, L. V., Allen, S. K., Bindoff, N. L., Bréon, F.-M., Church, J. A., Cubash, U., Emori, S., Forster, P., Friedlingstein, P., Talley, L. D., Vaughan, D. G., and Xie, S.-P.: Technical Summary, in: *Climate Change 2013: The Physical Science Basis. Contribution of Working Group I to the Fifth Assessment Report of the Intergovernmental Panel on Climate Change*, edited by: Stocker, T. F., Qin, D., Plattner, G.-K., Tignor, M., Allen, S. K., Boschung, J., Nauels, A., Y. Xia, V. B., and Midgley, P. M., Cambridge University Press, Cambridge, United Kingdom and New York, NY, USA., 33–115, <https://doi.org/10.1017/CBO9781107415324.005>, 2013.

937 Syvitski, J. P. M., Kettner, A. J., Overeem, I., Hutton, E. W. H., Hannon, M. T., Brakenridge, G. R., Day, J.,  
 938 Vörösmarty, C., Saito, Y., Giosan, L., and Nicholls, R. J.: Sinking deltas due to human activities, *Nat. Geosci.*,  
 939 <https://doi.org/10.1038/ngeo629>, 2009.  
 940 Teatini, P., Ferronato, M., Gambolati, G., Bertoni, W., and Gonella, M.: A century of land subsidence in  
 941 Ravenna, Italy, *Environ. Geol.*, 47, 831–846, <https://doi.org/10.1007/s00254-004-1215-9>, 2005.  
 942 Teatini, P., Ferronato, M., Gambolati, G., and Gonella, M.: Groundwater pumping and land subsidence in  
 943 the Emilia-Romagna coastland, Italy: Modeling the past occurrence and the future trend, *Water Resour. Res.*,  
 944 42, <https://doi.org/10.1029/2005WR004242>, 2006.  
 945 Teng, J., Jakeman, A. J., Vaze, J., Croke, B. F. W., Dutta, D., and Kim, S.: Flood inundation modelling: A  
 946 review of methods, recent advances and uncertainty analysis, <https://doi.org/10.1016/j.envsoft.2017.01.006>, 1  
 947 April 2017.  
 948 Tsimplis, M. N. and Rixen, M.: Sea level in the Mediterranean Sea: The contribution of temperature and  
 949 salinity changes, *Geophys. Res. Lett.*, 29, 51-1-51-4, <https://doi.org/10.1029/2002gl015870>, 2002.  
 950 Tsimplis, M. N., Marcos, M., and Somot, S.: 21st century Mediterranean sea level rise: Steric and atmospheric  
 951 pressure contributions from a regional model, *Glob. Planet. Change*, 63, 105–111,  
 952 <https://doi.org/10.1016/j.gloplacha.2007.09.006>, 2008.  
 953 Tsimplis, M. N., Raicich, F., Fenoglio-Marc, L., Shaw, A. G. P., Marcos, M., Somot, S., and Bergamasco, A.:  
 954 Recent developments in understanding sea level rise at the Adriatic coasts, *Phys. Chem. Earth*, 40–41, 59–71,  
 955 <https://doi.org/10.1016/j.pce.2009.11.007>, 2012.  
 956 Umgiesser, G., Bajo, M., Ferrarin, C., Cucco, A., Lionello, P., Zanchettin, D., Papa, A., Tosoni, A., Ferla, M.,  
 957 Coraci, E., Morucci, S., Crosato, F., Bonometto, A., Valentini, A., Orlic, M., Haigh, I., Nielsen, J. W., Bertin, X.,  
 958 Fortunato, A. B., Pérez Gómez, B., Alvarez Fanjul, E., Paradis, D., Jourdan, D., Pasquet, A., Murre, B.,  
 959 Tintoré, J., and Nicholls, R.: The prediction of floods in Venice: methods, models and uncertainty, *Nat.*  
 960 *Hazards Earth Syst. Sci.*, 1–47, <https://doi.org/10.5194/nhess-2020-361>, 2020.  
 961 Vousedoukas, M. I., Voukouvalas, E., Mentaschi, L., Dottori, F., Giardino, A., Bouziotas, D., Bianchi, A.,  
 962 Salamon, P., and Feyen, L.: Developments in large-scale coastal flood hazard mapping, *Nat. Hazards Earth*  
 963 *Syst. Sci.*, 16, 1841–1853, <https://doi.org/10.5194/nhess-16-1841-2016>, 2016.  
 964 Vousedoukas, M. I., Mentaschi, L., Feyen, L., and Voukouvalas, E.: Extreme sea levels on the rise along  
 965 Europe’s coasts, *Earth’s Futur.*, 5, 1–20, <https://doi.org/10.1002/ef2.192>, 2017.  
 966 Vousedoukas, M. I., Mentaschi, L., Voukouvalas, E., Verlaan, M., Jevrejeva, S., Jackson, L. P., and Feyen, L.:  
 967 Global probabilistic projections of extreme sea levels show intensification of coastal flood hazard, *Nat.*  
 968 *Commun.*, 9, 1–12, <https://doi.org/10.1038/s41467-018-04692-w>, 2018.  
 969 Wang, S., Najafi, M. R., Cannon, A. J., and Khan, A. A.: Uncertainties in Riverine and Coastal Flood Impacts  
 970 under Climate Change, 13, 1774, <https://doi.org/10.3390/w13131774>, 2021.  
 971 Wöppelmann, G. and Marcos, M.: Coastal sea level rise in southern Europe and the nonclimate contribution  
 972 of vertical land motion, *J. Geophys. Res. Ocean.*, 117, <https://doi.org/10.1029/2011JC007469>, 2012.  
 973 Zanchettin, D., Traverso, P., and Tomasino, M.: Observations on future sea level changes in the Venice  
 974 lagoon, *Hydrobiologia*, <https://doi.org/10.1007/s10750-006-0416-5>, 2007.  
 975 Zanchettin, D., Bruni, S., Raicich, F., Lionello, P., Adloff, F., Androssov, A., Antonioli, F., Artale, V.,  
 976 Carminati, E., Ferrarin, C., Fofonova, V., Nicholls, R., Rubinetti, S., Rubino, A., Sannino, G., Spada, G.,  
 977 Thiéblemont, R., Tsimplis, M., Umgiesser, G., Vignudelli, S., Wöppelmann, G., and Zerbini, S.: Review  
 978 article: Sea-level rise in Venice: historic and future trends, *Nat. Hazards Earth Syst. Sci. Discuss.*, 1–56,  
 979 <https://doi.org/10.5194/nhess-2020-351>, 2020.

## Annex 1

Here, we present the equations and the graphical results of the theoretical ESL scenarios. TWL results from the combination of storm surge, tide, and wave setup components, each following a general functional form (i.e. harmonic component) describing the oscillation of water level, following trigonometric functional forms for each component. These function equations are given as follows.

$$T_l = T_{max} \times \cos\left(2\pi \frac{1}{T_p} \times (t + T_d + T_p)\right) \quad \text{Eq. A1.1}$$

Where  $T_l$  is the tide level in meters at any given time,  $T_{max}$  is the maximum tide level in meters,  $T_p$  is the tidal period in seconds,  $T_d$  is the tidal period shift in time in seconds (used to match the peaks of tides and storm surge events), and  $t$  is the time in seconds.

$$SS = SS_{max} \times 0.5 \times \left(1 + \cos\left(2\pi \frac{1}{S_p} \times (t + S_d + S_p)\right)\right) \quad \text{Eq. A1.2}$$

Where  $SS$  is the storm surge level in meters at any given time,  $SS_{max}$  is the maximum storm surge level in meters,  $S_p$  is the storm surge duration in seconds,  $S_d$  is the storm surge shift in time in seconds (used to match the peaks of tides and storm surge events), and  $t$  is the time in seconds.

$$W_{s,int} = 0.5 \times \left(1 + \cos\left(2\pi \frac{1}{S_p} \times (t + S_d + S_p)\right)\right) \quad \text{Eq. A1.3}$$

$$W_s = W_{max} \times 0.5 \times \left(1 + \cos\left(2\pi \frac{1}{W_p} \times \left(t + \frac{W_p}{4}\right)\right)\right) \times W_{s,int} \quad \text{Eq. A1.4}$$

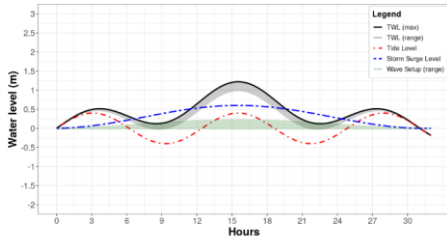
Where  $W_s$  is the wave setup level in meters at any given time,  $W_{max}$  is the maximum wave setup level in meters,  $W_p$  is the wave period in seconds,  $W_{s,int}$  is the intensity factor [0-1] of the wave setup event as a function of the storm surge intensity,  $S_p$  is the storm surge duration in seconds,  $S_d$  is the storm surge shift in time in seconds (used to match the peaks of tides and storm surge events), and  $t$  is the time in seconds.

We consider the wave setup component as a function of the intensity of the storm surge level, as shown in Eqs. A1.3 and A1.4. As such, wave setup is simulated as composite function, where the maximum wave setup level is designed to coincide in time with the maximum storm tide level, and the directions of the waves are set to coincide with the direction of the storm surge event, in our case, perpendicular to the coastline. This is done first to follow the assumption of worst-case scenario, and second to incorporate the flood dynamics resulting from the momentum of waves directed inlands. The composite function that combines Eqs. A1.1 to A1.4 and the effects of VLM and MSL (e.g. due to SLR) is shown in Eq. A1.5. The results of each component in Eqs. A1.1 to A1.4 and for each probabilistic scenario are shown in Figure A1.

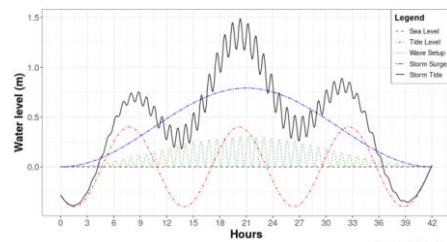
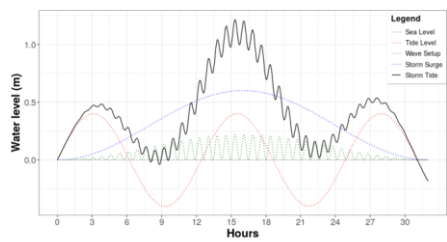
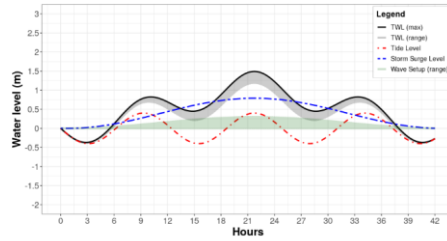
$$TWL = MSL + VLM + T_l + SS + W_s \quad \text{Eq. A1.5}$$



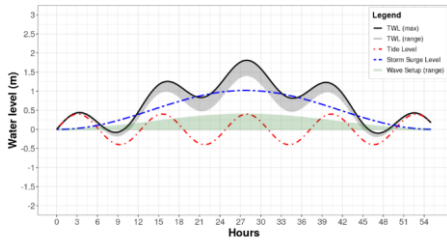
### RP 1 year



### RP 10 years



### RP 100 years



### RP 250 years

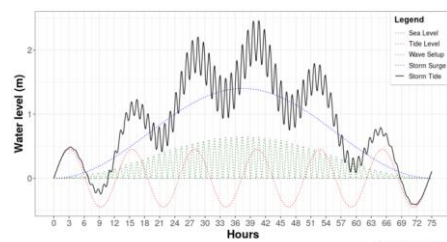
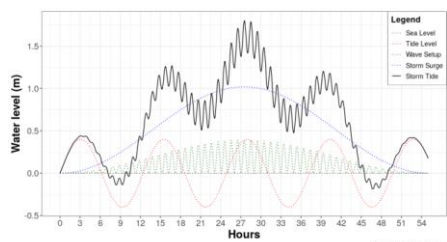
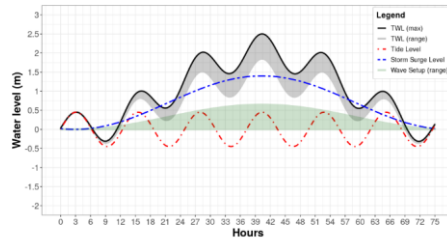
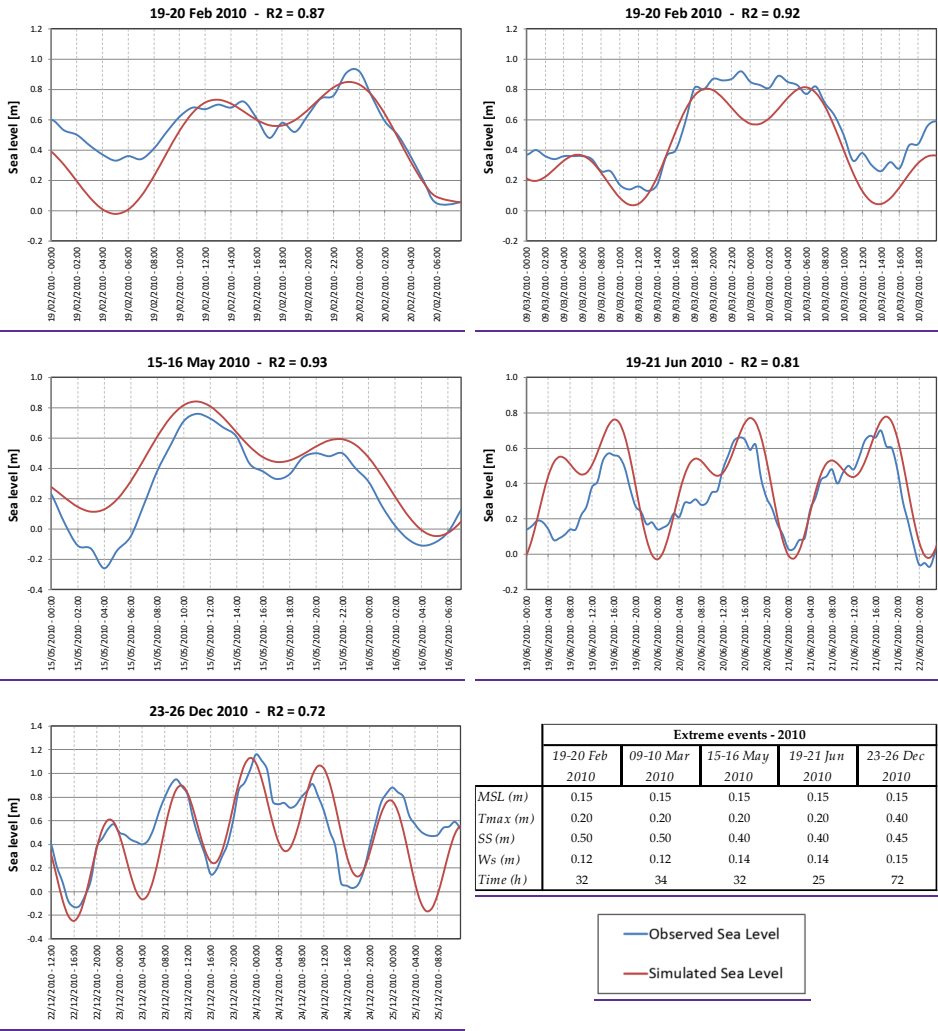


**Figure A1.** Dynamic boundary conditions for simulating theoretical extreme sea level events in ANUGA. The Total Water Level is shown as the grey shaded area, while the maximum Total Water Level is shown by the black line, at any given time. The tide (dashed red line), storm surge (dashed blue line) and wave setup (green shaded area) components define the total water level. Configurations are shown for the return periods of once-in-1, 10, 100 and 250 years.

In order to verify the applicability of the aforementioned functions, we test the methods explained in this annex for all five ESL events that were observed along the coastline of the ER region during the year 2010, as reported in (Perini et al., (2011)). Observed sea level data is obtained from ISPRA, for the station Ravenna –

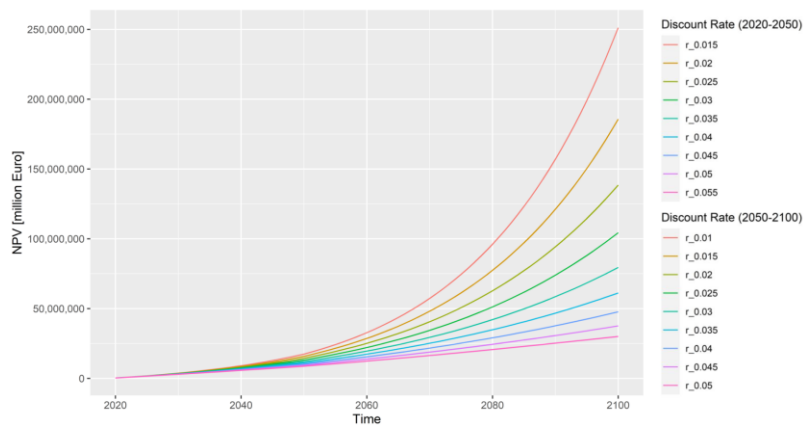
1015 [Porto Corsini](#) (Rete Mareografica Nazionale, 2021). We evaluate the goodness-of-fit of the methods by means  
1016 of Coefficient of determination (R2). The results of this analysis are shown in Figure A2 below.

1017



**Figure A2.** Comparison of the observed sea level (in blue) versus the simulated sea level using the harmonic components (in red).

1021 **Annex 12**  
1022 A sensitivity analysis is carried out on the discount rate. Figure A42 below shows how the NPV changes with  
1023 discount rate  $r$  ranging from 1.5% to 5.5% (2020 to 2050) and 1% to 5% (2050-2100).



1024 **Figure A24.** Sensitivity analysis of NPV using a variable discount rate.  
1025